Acta Pharmaceutica Sinica B 2025;15(5):2511−2528

Chinese Pharmaceutical Association
Institute of Materia Medica, Chinese Academy of Medical Sciences

Acta Pharmaceutica Sinica B

www.elsevier.com/locate/apsb
www.sciencedirect.com

ORIGINAL ARTICLE

A critical role for *Phocaeicola vulgatus* in negatively impacting metformin response in diabetes

Manyun Chen[a,b,c,d], Yilei Peng[a,b,c,d], Yuhui Hu[a,b,c,d], Zhiqiang Kang[e], Ting Chen[f], Yulong Zhang[a,b,c,d], Xiaoping Chen[a,b,c,d], Qing Li[a,b,c,d], Zuyi Yuan[g], Yue Wu[g], Heng Xu[h], Gan Zhou[a,b,c,d], Tao Liu[i], Honghao Zhou[a,b,c,d], Chunsu Yuan[j], Weihua Huang[a,b,c,d,*], Wei Zhang[a,b,c,d,*]

[a]*Department of Clinical Pharmacology, Xiangya Hospital, Central South University, Changsha 410008, China*
[b]*Engineering Research Center of Applied Technology of Pharmacogenomics, Ministry of Education, Changsha 410078, China*
[c]*Hunan Key Laboratory of Pharmacomicrobiomics, Changsha 410078, China*
[d]*National Clinical Research Center for Geriatric Disorders, Changsha 410008, China*
[e]*Zhengzhou Central Hospital Affiliated to Zhengzhou University, Zhengzhou University, Zhengzhou 450007, China*
[f]*Key Laboratory of Hunan Province for Integrated Traditional Chinese and Western Medicine on Prevention and Treatment of Cardio-Cerebral Diseases, Hunan University of Chinese Medicine, Changsha 410208, China*
[g]*Department of Cardiology, Cardiovascular Research Center, First Affiliated Hospital of Xi'an Jiaotong University, Xi'an 710061, China*
[h]*Department of Laboratory Medicine, National Key Laboratory of Biotherapy/ Collaborative Innovation Center of Biotherapy and Cancer Center, West China Hospital, Sichuan University, Chengdu 610041, China*
[i]*Shenzhen Center for Chronic Disease Control and Prevention, Shenzhen 518020, China*
[j]*Department of Anesthesia and Critical Care, University of Chicago, Chicago, IL 60637, USA*

Received 21 August 2024; received in revised form 28 December 2024; accepted 30 December 2024

KEY WORDS

Metformin resistance;
Ceramide;
Mitochondrial

Abstract Metformin has been demonstrated to attenuate hyperglycaemia by modulating the gut microbiota. However, the mechanisms through which the microbiome mediates metformin monotherapy failure (MMF) are unclear. Herein, in a prospective clinical cohort study of newly diagnosed type 2 diabetes mellitus (T2DM) patients treated with metformin monotherapy, metagenomic sequencing of faecal samples

*Corresponding authors.
E-mail addresses: csuzhangwei@csu.edu.cn (Wei Zhang), endeavor34852@csu.edu.cn (Weihua Huang).

Peer review under the responsibility of Chinese Pharmaceutical Association and Institute of Materia Medica, Chinese Academy of Medical Sciences.

https://doi.org/10.1016/j.apsb.2025.02.008

dysfunction;
Oxidative phosphorylation;
Gut microbiota;
Farnesoid X receptor;
Deconjugated bile acids;
Thermogenesis

revealed that *Phocaeicola vulgatus* abundance was approximately 12 times higher in nonresponders than in responders. *P. vulgatus* rapidly hydrolysed taurine-conjugated bile acids, leading to ceramide accumulation and reversing the improvements in glucose intolerance conferred by metformin in high-fat diet-fed mice. Interestingly, C22:0 ceramide bound to mitochondrial fission factor to induce mitochondrial fragmentation and impair hepatic oxidative phosphorylation in *P. vulgatus*-colonized hyperglycaemic mice, which could be exacerbated by metformin. This work suggests that metformin may be unsuitable for *P. vulgatus*-rich T2DM patients and that clinicians should be aware of metformin toxicity to mitochondria. Suppressing *P. vulgatus* growth with cefaclor or improving mitochondrial function using adenosylcobalamin may represent simple, safe, effective therapeutic strategies for addressing MMF.

1. Introduction

Metformin (MET) is the first-line drug for type 2 diabetes mellitus (T2DM) patients due to its safety, effectiveness, and cost advantage[1]. However, approximately 35% of patients on metformin monotherapy fail to achieve initial glycaemic control, and this metformin monotherapy failure (MMF) limits the widespread clinical use of this treatment[2]. Moreover, compared with metformin monotherapy, the combination of metformin with insulin or sulfonylureas increases the absolute risk of hypoglycaemia by approximately 10%[3]. Therefore, there is a clinical need to improve the effectiveness of metformin monotherapy.

The individual variation in the effects of metformin monotherapy on the hyperglycaemic response cannot be well explained by pharmacogenetics or pharmacokinetics[4−7]. Recently, the mechanism through which metformin monotherapy mediates hyperglycaemic control has been demonstrated to be significantly associated with the gut microbiota[8]. For example, the phenotype of blood sugar normalization by metformin can be transferred to germ-free mice fed a high-fat diet (HFD) through microbiota transplantation from metformin-treated mice, suggesting that the gut microbiota may influence the therapeutic response to metformin[9]. Additionally, with approximately 30% dose recovery of unchanged metformin from faeces, metformin has been shown to reprogram the disordered microbial communities in T2DM patients, specifically by increasing the abundance of species such as *Lactobacillus* spp., *Bifidobacterium* spp. and *Akkermansia* spp.[9−11]. Increased levels of microbial metabolites such as short-chain fatty acids (SCFAs) could activate G-protein-coupled receptors (such as free fatty acid receptors 2 and 3) on intestinal L-cells and promote the secretion of glucagon-like peptide-I to regulate blood sugar[12]. However, the ability of bacteria to attenuate the efficacy of metformin has attracted less attention than the effects of metformin on the microbiota.

In this context, it has been shown that imidazole propionate, a microbially-produced histidine-derived metabolite, can weaken metformin efficacy by activating p38γ, which then inhibits adenosine 5′-monophosphate (AMP)-activated protein kinase (AMPK)[13]. However, the hypoglycaemic effect of metformin is maintained in mice lacking AMPK in the liver[14], implying that other mechanisms independent of AMPK are involved. For example, *Bacteroides fragilis* significantly abrogates the anti-hyperglycaemic effect of metformin by inducing metabolic dysfunction *via* the bile salt hydrolase (BSH)−bile acid (BA)−farnesoid X receptor (FXR) axis[10]. However, *B. fragilis* levels are decreased in faecal samples collected from naïve T2DM patients treated with metformin for 3 days. Therefore, suppressing *B. fragilis* is likely not sufficient to cause MMF. Furthermore, there is very little data on the relationship between long-term MMF and specific bacteria inhabiting the intestine.

As a metabolic regulator, FXR regulates the intestinal bile acid pool (FXR/Fibroblast growth factor 15 axis)[15], intestinal lipid absorption (FXR/small heterodimer partner (SHP)/sterol regulatory element-binding protein 1c (SREBP1c) pathway)[16], glucose metabolism and energy metabolism (FXR/peroxisome proliferator-activated receptor γ (PPARγ)/fatty acid oxidation axis)[17]. Regarding the regulation of glucose metabolism, the intestinal FXR-specific inhibitor was able to reduce insulin resistance in HFD-fed mice as a result of decreased expression of proteins involved in ceramide synthesis, which reduced intestinal and serum ceramide levels[18]. As a major determinant of lipotoxicity, ceramides promote weight gain and glucose intolerance. Recent studies of animals have indicated that high ceramide levels are associated with mitochondrial fragmentation through the mitochondrial fission factor (MFF)/dynamin-related protein 1 (DRP1) pathway in obesity[19] or activation of protein phosphatase 2A to impede clearance of dysfunctional mitochondria in acute kidney injury[20]. Once fragmented, the mitochondrial electron transport chain (ETC) and oxidative phosphorylation (OXPHOS) are impaired to reduce ATP synthesis and consumption of direct energy substrates (*e.g.*, glucose and lactate). It is clear that microbial-derived secondary BAs, such as chenodeoxycholic acid (CDCA), ursodeoxycholic acid (UDCA), 7-ketodeoxycholic acid (7-keto-DCA), deoxycholic acid (DCA) and lithocholic acid (LCA), play an important role in the regulation of hepatic glycolipid metabolism as endogenous FXR ligands[21,22]. However, an in-depth understanding of the role of microbial-derived bile, sphingolipids, and mitochondrial fragmentation in the regulation of metformin action is lacking.

To address the unresolved questions noted above, we performed detailed metagenomic sequencing and metabolomics analyses of drug-naïve patients with type 2 diabetes who did or did not respond to metformin treatment for 3 months to reveal the mechanisms of gut microbiota-driven MMF. We found that the relative abundance of the gut commensal *Phocaeicola vulgatus* in the faecal samples of patients with MMF was markedly increased. Colonization of HFD-fed mice with the faecal microbiota of nonresponders and *P. vulgatus* impaired the ability of metformin to improve glucose control due to the inhibition of hepatic cholesterol catabolism and the promotion of ceramide biosynthesis mediated by FXR. Furthermore, increased sphingolipid

levels enhanced the mitochondrial toxicity of metformin, which induced hepatic mitochondrial fragmentation and decreased adipose thermogenesis. Reduced consumption of glucose as an energy substrate and impaired fatty acid beta-oxidation led to a net positive energy balance in HFD-fed mice, ultimately undermining the beneficial effects of metformin on metabolic disease. Thus, this study establishes a stable metformin resistance model involving the gut microbiota. The results suggest that suppressing intestinal FXR activation, BSH activity, and *P. vulgatus* abundance using cefaclor or improving mitochondrial function with vitamin B12 (VB12) are potential approaches for reversing the lack of response to metformin in nonresponders.

2. Materials and methods

2.1. Human subjects

All participants provided written informed consent. Chinese Han patients with naïve T2DM were recruited for the study according to strict inclusion and exclusion criteria. All participants received diabetes education, anthropometrics, metabolic assessments, and biochemical assays.

Participants received oral metformin hydrochloride treatment (1000 mg for 1−2 weeks, then 2000 mg per day, Sino-American Shanghai Squibb Pharmaceuticals Ltd.). All participants attended a follow-up visit once a month. In 12 weeks, participants were assigned to the nonresponder group (7.0 mmol/L $<$ fasting blood glucose (FBG) $<$ 13.3 mmol/L or hemoglobin A1c (HbA1c) $\geq$ 7%) or to the responder group (FBG $<$7.0 mmol/L and HbA1c $<$ 7%). Anthropometric measurements, biological samples (plasma and feces samples), and metabolic testing were carried out at the end-of-intervention term. The clinical trial was a prospective study in patients with T2DM (trial registration number from Chinese Clinical Trial Registry: ChiCTR1900022997). The study protocol was approved by the Medical Ethics Committee of Xiangya Hospital, Central South University (ID: 2019040116), and conducted in accordance with the principles of the Declaration of Helsinki.

2.2. Human gut microbiota DNA extraction and metagenomics sequencing

Fecal genomic DNA was extracted using a Magnetic Soil and Stool DNA kit (Tiangen, Beijing, China) and sequenced on the Illumina Novaseq platform (150 bp; paired-end).

2.3. The quantification of metformin in human plasma and bile acids quantification

For metformin and bile acids quantification, human fecal and plasma samples were analyzed using highly sensitive and selective ultra-performance liquid chromatography coupled to a tandem mass spectrometry (UPLC−MS/MS) method. The MS/MS parameters optimized for the method are showed in Supporting Information Tables S1−S5.

2.4. P. vulgatus culture and a high-throughput growth curves screen on gut bacteria

P. vulgatus (ATCC 8482) was streaked onto a Brain-Heart Infusion (BHI, OXOID, Cambridge, UK) agar plate in an anaerobic workstation (10% CO_2, 10% H_2 and 80% N_2) at 37 °C for 48 h. Bacteria were cultured in anaerobic tubes in the presence or absence of metformin (40 μmol/L, 1.5 and 10 mmol/L). OD_{600} values were measured hourly.

For colonization of bacteria, *P. vulgatus* suspended in 200 μL of anaerobic PBS (5.0×10^8 colony-forming units per mouse) or the same dosage of heat-killed bacteria (pasteurization, 60 °C for 20 min) were orally administered to mice daily.

2.5. RNA sequencing and analysis

Total RNA was extracted from *P. vulgatus* or mouse liver tissue using RNeasy Protect Bacteria Mini Kit (QIAGEN, CA, USA) or TRIzol reagent (Invitrogen, CA, USA), and sequenced on the Illumina Novaseq 6000 platform (150 bp; paired-end).

2.6. Animals

Male mice were housed in a pathogen-free animal facility under alternating 12 h light and dark cycles and given free access to food and water. C57BL/6J mice (aged 6 weeks) were fed a high-fat diet HFD (60% kcal from fat, D12492, Research Diets, NJ, USA) for 14 weeks, compared them with normal chow diet (ND) fed mice. The mice were fed an antibiotics cocktail consisting of vancomycin 50 mg/kg, neomycin 100 mg/kg, metronidazole 100 mg/kg, amphotericin-B 1 mg/kg, and ampicillin 1 mg/mL for 7 days. The gut microbiota-depleted mice were transplanted with fecal microbiota from responders or nonresponders, *P. vulgatus* or heat-killed *P. vulgatus* (HK−*P. vulgatus*) under HFD treatment for 4 weeks continuously. *db*/*db* mice (aged 5 weeks) were fed a standard chow diet. BAs were orally administrated in *db*/*db* mice.

Animals were anaesthetized with isoflurane to collect blood samples by retro-orbital sinus puncture. Other specimens (liver, ileum, ileal contents, and adipose) were collected and stored at −80 °C until analysis.

The experimental procedures were performed in compliance with Laboratory Animal Center of Central South University guidelines and approved by the Institutional Animal Care and Use Committee (No. 2020sydw0814).

2.7. Fecal microbiota preparation

Stool samples collected from 5 responder donors or 5 nonresponder donors were mixed together for fecal microbiota transplantation (FMT), respectively. One gram of fecal sample was suspended in 20 mL of Ren's solution containing 10% skimmed milk, and then aliquoted and stored at −80 °C. Mice were given 200 μL of fecal microbiota by gavage each day for 4 weeks.

2.8. Animal gut microbiota DNA extraction and 16S rRNA gene amplicon sequencing

The intestinal microbial composition was examined whether faecal microbiota transplant from responder or nonresponder donors into recipient mice by 16S sequencing. Faeces from mice were collected on Day 28 during FMT. Fecal genomic DNA of human donors and mice recipients were extracted using cetyltrimethyl ammonium bromide method. Bacterial 16S rRNA gene amplicon paired-end sequencing was performed on the Illumina Novaseq 6000 platform (250 bp; paired-end reads; mean of 70,000 effective Tags/samples).

2.9. Oral glucose tolerance testing (OGTT), insulin tolerance testing (ITT) and HOMA-IR

OGTT was performed using oral gavage of glucose at 2 g/kg body weight for C57BL/6J mice or 1 g/kg for *db*/*db* mice after 6 h or 12 h of fasting. ITT was performed using i.p. injection of insulin at 0.75 U/kg body weight for C57BL/6J mice after 4 h of fasting. Blood glucose concentrations were measured using a glucometer (Accu-Chek Active, Roche Diagnostics, Mannheim, Germany; αTRAK2, αTRAK, Chicago, IL, USA). Plasma insulin concentrations were measured using the Ultra-Sensitive Mouse Insulin ELISA Kit (Crystal Chem, Downers Grove, IL, USA). HOMA-IR was calculated according to Eq. (1):

$$\text{HOMA-IR} = \text{Fasting insulin (microIU/L)} \times \text{Fasting glucose (nmol/L)}/22.5 \quad (1)$$

2.10. Histological analysis

Liver tissues were fixed in 4% paraformaldehyde and stained by oil red O (ORO) and periodic acid-Schiff (PAS) staining. Adipose tissues were fixed in 4% paraformaldehyde and stained by immunostaining with adiponectin antibody (Bioss, Cat# bs-0471R, 1:200), leptin antibody (ImmunoWay, Cat# YT3226, 1:200) for subcutaneous fat, and visfatin antibody (Bioss, Cat# bs-10245R, 1:200) for epididymal fat. The adipose tissues sections were also stained with hematoxylin and eosin (H&E). For immunofluorescence staining, slides were incubated with insulin (Proteintech, Cat# 15848-1-AP, 1:100) and glucagon (Proteintech, Cat# 67286-1-Ig, 1:200) antibody and counterstained with DAPI to obtain images.

2.11. RNA isolation and RT-qPCR analysis

RNA was extracted from tissues with Trizol reagent using a standard chloroform-isoamyl alcohol extraction. 1 μg of total RNA was reverse-transcribed using a transcription kit according to the manufacturer's instructions. Relative mRNA expression levels were determined by qPCR using the QuantStudio 5 Real-Time PCR system. The primers used for RT-qPCR are provided in Supporting Information Table S6.

2.12. Western blot analysis and capillary-based Western blot

Tissues were homogenized in Tissue Protein Extraction Reagent with protease and phosphatase inhibitors. Protein was separated by SDS-PAGE electrophoresis and transferred to a PVDF membrane. The membrane was incubated with primary antibodies against FXR (Cell Signaling Technology, Cat# 72105, 1:1000), CYP7B1 (Proteintech, Cat# 24889-1-AP, 1:600), CYP7A1 (Abcam, Cat# ab65596, 1:1000), SHP (Absin, Cat# abs115798, 1:1000) or GAPDH (Cell Signaling Technology, Cat# 2118, 1:20,000) overnight at 4 °C.

We also used an automated capillary Western blot (Jess, Protein Simple). The primary antibodies were DRP1 (Cell Signaling Technology, Cat# 8570S, 1:30), Phospho-DRP1 (Ser616) (Cell Signaling Technology, Cat# 4494S, 1:10) and SREBF1 (Proteintech, Cat# 14088-1-AP, 1:10). Chemiluminescence data were produced by the Compass for SW software (version 6.2.0, Protein Simple). All values were normalized to GAPDH (Cell Signaling Technology, Cat# 2118, 1:750).

2.13. Mitochondrial membrane potential assay

The change of mitochondrial membrane potential of hepatic tissue was assayed by using JC-10 Mitochondrial Membrane Potential Assay Kit (Solarbio, Beijing, China). JC-10 staining was detected by a fluorescent reader under Ex_{490}/Em_{530} for monomer and Ex_{525}/Em_{590} for polymer (Aggregate). The ratio of aggregates/monomers suggested the dissipation of mitochondrial transmembrane potential and data were relative to vehicle/control. CCCP (5 μmol/L) was applied as a positive control inducing JC-10 depolymerization.

HepG2 cells were loaded with 200 nmol/L MitoTracker Red CMXRos for 30 min. Coverslips were mounted in mounting medium with DAPI; cells were visualized under a fluorescence microscope and processed using ImageJ (Fiji) software.

2.14. Transmission electron microscopy

1 mm^3 of liver section from mice were fixed in 0.2 mol/L phosphate buffer (KH_2PO_4/Na_2HPO_4, pH 7.5) supplemented with 2.5% glutaraldehyde for at least 24 h at 4 °C. Ultrathin sections (50−100 nm) were cut, and then contrasted with 3% uranyl acetate and lead nitrate. Images were acquired with a transmission electron microscope (Hitachi H7700). Mitochondrial aspect ratio (calculated by major axis/minor axis) were measured using ImageJ (Fiji)-software.

2.15. Measurement of mtDNA-CN

Total DNA was isolated from stored tissue by using DNeasy Blood and Tissue Kit (QIAGEN, CA, USA). The amount of mtDNA (mt−*Nd1*) and nuclear-encoded gene (*nGADPH*) were quantified were calculated using droplet digital PCR (ddPCR) (Bio-Rad Laboratories, CA, USA). The mtDNA-CN was represented as the ratio between the number of mt−*Nd1* copies/μL and the number of *nGADPH* copies/μL.

2.16. The surface plasmon resonance (SPR) assay

Affinity and K_D measurements were performed using a Biacore 8K+. The CM5 Sensor Chip (Cytiva, MA, USA) was used to couple the recombinant Human MFF protein (Novus Biologicals, CO, USA), and the running buffer was PBS with 2% ethanol. The protein was coupled to a CM5 chip with approximately 15,000 RU coupling amount for each channel. Proteins were diluted with 10 mmol/L sodium acetate buffer (pH 5.0). For evaluation of the affinity, Cer(18:1/22:0) and Cer(18:1/22:1) (Cayman Chemical, MI, USA) were diluted to 100 μmol/L. For evaluation of the K_D value, Cer(18:1/16:0) was from 25 to 0.78125 μmol/L. All data processing was performed in the Biacore 8K + analysis software.

2.17. In vitro treatment of ceramides

HepG2 cells were plated into 12-well culture plates at 2×10^5 cells per well for 24 h. After adhesion, cells were treated with an oleate/palmitate mixture (2:1 mol/mol ratio, 0.75 mmol/L as the final concentration) in combination with 10 mmol/L sucrose in glucose-free DMEM supplemented with 2 mmol/L GlutaMAX and 1 mmol/L sodium pyruvate for 72 h. Cells were then treated with either ethanol (vehicle), ceramide (d18:1/22:0), ceramide (d18:1/22:1) or ceramide (d18:1/16:0) for 24 h in glucose-free

DMEM supplemented with 2 mmol/L GlutaMAX and 1 g/L glucose as MEM.

2.18. Seahorse extracellular flux measurement

HepG2 cells were seeded in an XF 96 Well Plate at 3×10^3 cells/well for 24 h, followed by the treatment as described above. On the day of the assay, cells were washed one time with PBS and media was replaced with Seahorse XF base medium containing 10 mmol/L glucose, 1 mmol/L sodium pyruvate and 2 mmol/L glutamine. After incubating in a non-CO_2 incubator at 37 °C for 1 h, the cell plate was inserted into a Seahorse XF 96 Analyzer (Agilent Technologies, CA, USA) After 3 basal measurements, oligomycin was injected for a final concentration of 1.5 mmol/L to inhibit ATP synthesis. Next, FCCP was injected with a final concentration of 1 mmol/L to determine maximal respiratory capacity. Finally, a mixture of rotenone and antimycin was injected to inhibit all mitochondrial respiration (final concentration of 0.5 mmol/L each). Protein concentration of the cells or cell number was measured after the analysis and used to normalize the oxygen consumption rate (OCR).

2.19. Statistical analysis

GraphPad Prism version 8.0, IBM SPSS Statistics 26 and R (version 3.5.1 and 4.2.0) were used for statistical analysis. Experimental data were shown as the mean ± standard error of mean (SEM) or mean ± standard deviation (SD). The sample size was estimated on the basis of previous experience, sample availability and previously reported studies. Unpaired independent Student's *t*-tests (between two groups) and one-way ANOVA with Tukey's or Dunnett's tests (among multiple groups) were used to compare differences upon normally distributed and homogeneous variances. Non-normally distributed or heterogeneous data were compared by the Mann−Whitney U tests (Wilcoxon rank-sum test, between two groups) or the Kruskal Wallis test (among multiple groups). A Benjamini−Hochberg adjusted *P*-value (FDR) of 0.05 was used as the cutoff for statistical significance unless stated otherwise. Correlation analysis of gut microbiome and subjects' clinical characteristics were investigated using Spearman's rank correlation coefficient test. Statistical significance is indicated by asterisks (*): $*P < 0.05$, $**P < 0.01$, $***P < 0.001$, $****P < 0.0001$, ns, non-significant.

3. Results

3.1. P. vulgatus is enriched in nonresponders after metformin treatment

To determine the relationship between the gut microbiome and metformin glycaemic response, we compared the gut microbiota compositions using faecal samples from 18 patients in the responder group (FBG <7.0 mmol/L and HbA1c < 7%) and 18 patients in the nonresponder group (7.0 mmol/L < FBG <13.3 mmol/L or HbA1c ≥ 7%) who were treated with metformin for 3 months. Responders and nonresponders were matched for features of plasma glucose homeostasis and other phenotypes using propensity score matching to minimize potential confounders, successfully completed the trial and provided enough faecal and plasma samples for analysis (CONSORT participant flow diagram see Supporting Information Fig. S1A). Clinical characteristics are shown in Supporting Information Table S7. Notably, no significant differences in clinical characteristics, including FBG levels andHbA1c, were observed between the groups at baseline (Fig. 1A). Moreover, the plasma levels of metformin were not significantly different at the end of the intervention (Fig. S1B). Although metformin caused a progressive decline in HbA1c levels, subjects in the nonresponder group had significantly higher FBG or HbA1c levels and failed to achieve the goal of tight glycaemic control, unlike those in the responder group, even though they did not initially have higher blood sugar levels. It is therefore unlikely that the observed differences in metformin responses stemed from a different glycaemic baseline.

One potential mechanism underlying MMF involves the alteration of the intestinal microbiome or microbial metabolites, which can affect metformin activity[10,13]. However, there is limited evidence that this mechanism mediates MMF, and available data are from short-term studies. To investigate whether the gut microbiota was different between the responders and nonresponders, we first performed whole-genome shotgun sequencing to explore the microbiome taxonomic identification *via* MetaPhlAn 4.0.6. Principal coordinate analysis (PCoA) revealed that the gut microbiota profile presented a clear alteration between the two groups (Fig. 1B). In metformin nonresponders, the relative abundance of Bacteroidetes was increased, while the relative abundances of Firmicutes and Actinobacteria were decreased at the phylum level (Fig. S1C). At the genus level, the abundances of *Bacteroides* spp. and *Phocaeicoia* spp. were significantly enhanced (Fig. S1D and S1E). Consistent with the species level (Fig. 1C), analysis with the linear discriminant analysis (LDA) effect size (LEfSe) method revealed that the nonresponder group was characterized by *P. vulgatus*, *B. uniformis*, *B. plebeius* and *B. ovatus* (Fig. 1D). Next, we used a random forest classifier to select the discriminating features in the gut microbiota for differentiating species, including *P. vulgatus* (Fig. S1F). Differential analyses were performed using MaAsLin2 and ALDEx2 with adjustment for covariates. Further evaluation of the microbiota confirmed the significant enrichment of *P. vulgatus* in the nonresponder group, which exhibited the highest relative abundance (approximately 11.96 times higher than that in the responder group) (Fig. S1G and Fig. 1E). In addition, it has been reported that patients with refractory diabetes show an increased relative abundance of *P. vulgatus* concomitant with a reduction in the abundance of the glucose homeostasis-related species *Akkermansia muciniphila*[23,24]. However, the relative abundance of *A. muciniphila* was not significantly different between the two groups in our study. Before metformin treatment, the nonresponder group was characterized by *Ruminococcus bromii*, *Alistipes onderdonkii*, *B. caccae* and *B. finegoldii*, while *Bifidobacterium. Longum*, *Veillonella. parvula* and *Streptococcus. salivarius* were enriched in the responder group (Fig. S1H). Thus, the abnormal alterations in the gut microbiota under metformin treatment may be related to the occurrence of MMF.

Gut microbiota functional gene profiles at the KO (Kyoto Encyclopedia of Genes and Genomes (KEGG) ortholog) level were also different between the two groups after metformin treatment (Fig. S1I). The differentially expressed bacterial genes are involved in glycan metabolism, lipoic acid biosynthesis and fatty acid biosynthesis (Fig. S1J). We mapped reads to carbohydrate-active enzymes (CAZymes) and found that 81 were significantly different between responders and nonresponders. Metformin led to a reduction in the levels of CAZymes involved in the biosynthesis of dextransucrase (CAZyme ID GH70) and an increase in the capacity to metabolize lactose (β-galactosidase

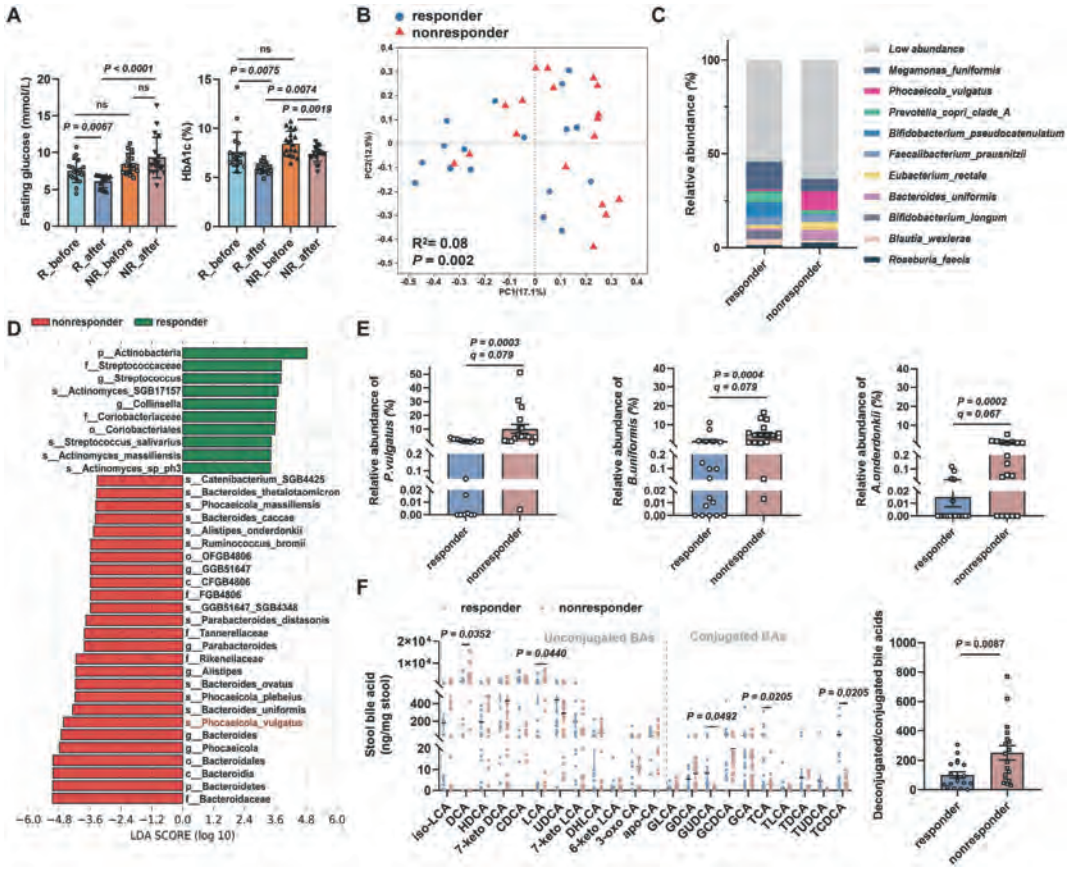

Figure 1 Metformin treatment induces different gut microbiota and bile acid metabolism changes in non-responders. (A) Fasting blood glucose and HbA1c levels of newly diagnosed T2DM patients before and after metformin treatment; R_before: responders before metformin treatment ($n = 18$); NR_before: nonresponders before metformin treatment ($n = 18$); R_after: responders after 3-month metformin treatments ($n = 18$); NR_after: nonresponders after 3-month metformin treatments ($n = 18$). (B) Principal coordinates analysis (PcoA) plot based on *Bray−Curtis* dissimilarity matrices in responders and nonresponders. The data were compared by the PERMANOVA test ($n = 18$). (C) Stacked bar plots showing the average percent relative abundances at the species level for responder and nonresponder groups, respectively. The most abundant taxa are shown as differently colored bars, with lower abundance taxa grouped as a gray bar (Others). (D) Differences in bacterial taxonomy were ranked according to the linear discriminant analysis (LDA) effect size between responders and nonresponders. (E) Abundance of *P. vulgatus, B. uniformis* and *A. onderdonkii* based on metagenomics data. Statistical significance is based on *P* values and *q* values obtained from MaAsLin2 analysis ($q < 0.1$). (F) Bile acid levels in stool samples; ratio of deconjugated BAs/conjugated BAs. *P* value determined by two-tailed unpaired Student's *t*-test, paired Student's *t*-test, Mann−Whitney U test and Kruskal−Wallis test. ns, non-significant. All data are presented as mean ± SEM or mean ± SD.

(GH147)) and plant cell wall degradation (pectate lyase (PL10)) in nonresponders (Fig. S1K). The relative expression of *cgh* (microbiome-encoded choloylglycine hydrolase, a kind of bile salt hydrolase) in the faecal microbiome of the nonresponder group was higher than that in the responder group (Supporting Information Fig. S2A), we next aimed to integrate bile acid metabolomic profiling, metagenomic sequencing and clinical monitoring. We analysed a panel of major BAs in faeces using UPLC−MS/MS and found that the unconjuagated BA levels, especially LCA (FXR agonist) and DCA (FXR agonist), were significantly higher in the metformin nonresponder group than in the responder group. The levels of conjugated BAs, such as glycoursodeoxycholic acid (GUDCA), taurochenodeoxycholic acid (TCDCA) and taurocholic acid (TCA), were markedly reduced. The levels of deconjugated BAs in the nonresponders after 3-month metformin treatments group were approximately 1.56 times higher and those of conjugated BAs were approximately 71.5% lower (Fig. 1F). Correlation analysis of faecal bacteria, BA and plasma glycolipid levels showed that the abundances of *Phocaeicola spp.*, *Bacteroides* spp. and *Alistipes* spp. were positively correlated with FBG and HbA1c levels, whereas the abundance of *Blautia* spp. and *Mediterraneibacter* spp. were negatively correlated with post prandial glucose levels. In terms of metabolic indicators, the ratio of deconjugated BAs to conjugated BAs was positively correlated with HOMA-IR and post prandial glucose (PPG) (Fig. S2B and S2C).

Together, these data reveal that even at the same dose and duration of metformin treatment, patients with similar initial blood glucose levels will still have different alterations in their gut microbiota at both the compositional and functional potential levels. Notably, *P. vulgatus* was significantly enriched in nonresponders after metformin treatment. In addition, unconjugated/conjugated BA transformation during metformin treatment accumulates in the intestine to a relatively large degree.

3.2. Glucose and metformin are beneficial in promoting the growth of P. vulgatus

To understand how individual strains in the gut ecosystem respond to metformin, we monitored the growth curves of 33 representative gut bacterial strains upon treatment with metformin (Supporting Information Fig. S3A). Metformin did not inhibit *P. vulgatus* growth and, in fact, improved the growth advantage in the stationary phase (Fig. S3B). To identify the distinct response of *P. vulgatus* to metformin, we performed RNA-seq analysis using *P. vulgatus* cultures. Among the total 3968 genes that were identified, 5 were upregulated and 11 were downregulated in the metformin-treated group compared with the control group (Fig. S3C). *BVU_1748* (encoding the two-component system sensor histidine kinase) was more highly expressed after metformin treatment. In addition, the mRNA levels of RNA polymerase sigma factor (*BVU_RS16825*) increased (Fig. S3D). Intriguingly, we uncovered the existence of an advantage conferred by growth regulations under metformin in response to carbon (C), nitrogen (N), and phosphate (P) limitations, especially glucose limitation (Fig. S3E). However, in the case of defined rich media with sufficient glucose, the growth-promoting effect of metformin is found to be relatively insignificant (Fig. S3F). Metformin may increase the sensitivity of *P. vulgatus* to changes in different environmental cues to regulate its survival and cellular development. Moreover, the concentration of lactate in non-responders was found to be significantly higher than in responders (Fig. S3G). The addition of L-lactate could significantly enhance the growth of *P. vulgatus in vitro* (Fig. S3H), consistent with previous reports[25]. Therefore, metformin increases *P. vulgatus* in non-responder, which may be attributed to the combined influence of the bacteria itself and the host's metabolic processes.

To elucidate the correlation between bile acid transformation and *P. vulgatus*, we then determined the efficiency of the hydrolysis of different BAs conjugated to glycine or taurine by *P. vulgatus*. Metformin could not reduce the efficiency of hydrolysis by *P. vulgatus* or the level of *bsh* mRNA (Fig. S3I). After incubation with *P. vulgatus* for 24 h, approximately 76.6% of tauroursodeoxycholic acid (TUDCA) was hydrolysed by *P. vulgatus* after 3 h glycolithocholic acid (GLCA), TCDCA and taurolithocholic acid (TLCA) were also rapidly metabolized (the ratio of remaining $\leq$80% within 3 h). However, more than 80% of glycochenodeoxycholic acid (GCDCA), glycocholic acid (GCA), glycodeoxycholic acid (GDCA), GUDCA, TCA, and taurodeoxycholic acid (TDCA) remained at 3 h (Fig. S3J and S3K). Taken together, these results suggest that *P. vulgatus* correlates with individual-specific variations in BA metabolism among nonresponders.

3.3. Responses to metformin monotherapy are attenuated after FMT from nonresponders

To determine whether FMT from nonresponder patients into mice could induce an MMF-like phenotype, we colonized microbiota-depleted HFD-fed mice with stool microbiomes collected from five members of the nonresponder group and five of the responder group. After one week of treatment with antibiotics (Supporting Information Fig. S4A), mice underwent microbial transplantation (Fig. 2A) each day for 4 weeks. Then, faecal samples were collected to confirm the FMT efficiency using 16S rRNA sequencing, and we found that FMT induced alterations in the gut microbiota (an increase in the relative abundances of *P. vulgatus*, *B. ovatus* and *B. uniformis* species, Fig. S4B), and the transferred functions of the faecal microbiota from each donor to every recipient group (Fig. S4C) were strongly similar to those of the MMF donors.

Strikingly, the glycaemic responses in the microbe-humanized mice largely reflected those of their donors. The hypoglycaemic effect of metformin, including lowered glucose tolerance and HOMA-IR, was attenuated after FMT from nonresponders but preserved after FMT from responders (Fig. 2B and C). In terms of insulin indicators, there was fewer β-cells in islets, and these β-cells were interspersed with a greater number of α-cells (Fig. 2D). Moreover, the index of adiposity, such as hepatic triglyceride (TG) levels, body weight, glucagon-like peptide-1 (GLP-1) levels and adipocyte size, was more serious in the FMT_{non} + MET group than in the group treated with metformin that did not undergo FMT (Fig. 2E−I).

Furthermore, the expression of hepatic *Fxr*, *Shp* (small heterodimer partner), and *Cyp7b1* (25-hydroxycholesterol 7-α-hydroxylase) was lower in mice that received nonresponder microbiota than in mice that received metformin without FMT (Fig. S4D−S4G). However, the expression of hepatic cholesterol 7α-hydroxylase (*Cyp7a1*) and sterol 12α-hydroxylase (*Cyp8b1*), key enzymes in the classic BA synthesis pathway, was not significantly decreased (Fig. S4H and S4I). Moreover, hepatic *Baat* (bile acid-CoA:amino acid *N*-acyltransferase) mRNA expression was decreased (Fig. S4J), suggesting the conjugation of primary BAs (cholic acid (CA) and CDCA) with glycine or taurine attenuation. The mRNA level of ileal pical sodium bile acid transporter (*Slc10a2*) was also significantly lower in the metformin group (Fig. S4K). The gene expression of hepatic sterol 27-hydroxylase (*Cyp27a1*) and ileal bile acid-binding protein (*Ibabp*) did not differ between the groups that received metformin with or without FMT (Fig. S4L and S4M).

Consistent with the above findings, *Bifidobacterium pseudocatenulatum*, a kind of probiotic that has been found to be negatively associated with T2DM[26], showed strong BSH activity (Fig. S4N) but could not improve the response to metformin (Fig. 2J−L) in nonresponder gut microbiota recipient mice. TG levels were negatively correlated with a suppressed hepatic FXR−SHP axis, which impairs hepatic gluconeogenesis and glucose homeostasis. These findings suggest that the *Phocaeicoia*-rich microbiota of nonresponding donors can induce the MMF phenotype and promote ileal BA absorption in recipients through hepatic feedback to inhibit BA synthesis.

3.4. P. vulgatus reverse the hypoglycaemic effect of metformin

Based on the aforementioned alterations, to clarify the detrimental effects of the *P. vulgatus*-rich microbiota on metformin activity, microbiota-depleted HFD-fed mice were gavaged with 10^8 CFU *P. vulgatus* every day for 4 weeks, and then mice were treated with metformin for two weeks (Fig. 3A; Supporting Information Fig. S5A). The beneficial effects of metformin, including lowering blood sugar, increasing insulin sensitivity, weight loss and improving lipid metabolism disorders, were lower in mice precolonized with *P. vulgatus* than in those precolonized with heat-killed *P. vulgatus* (HK−*P. vulgatus*, Fig. 3B−H). As key regulators of lipid metabolism, adipocytokines, including adiponectin, leptin and visfatin, were lower (Fig. 3I). Furthermore, the *P. vulgatus*-treated mice given metformin showed increases in hepatic TG levels and adipocytes of the subcutaneous fat (Fig. S5B and S5C). Deconjugated BA levels in plasma were measured;

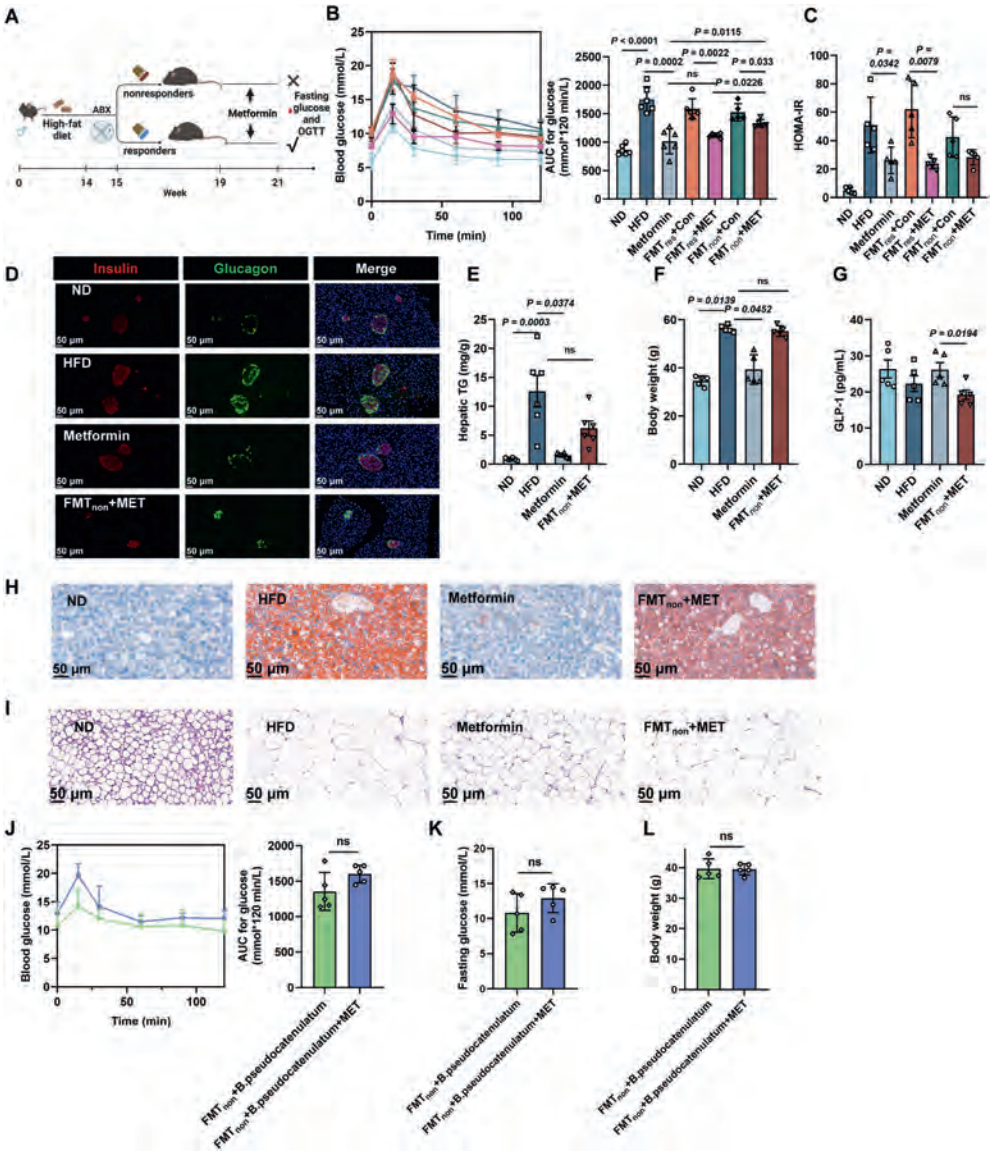

Figure 2 The beneficial effects of metformin were reduced in mouse recipients receiving nonresponders' fecal microbiota. (A) Experimental procedure for fecal microbiota transplantation (n = 5−6). (B) Oral glucose tolerance test (OGTT) and area under the curve (AUC) (n = 5−6). (C) HOMA-IR of mice treated with metformin or FMT (n = 5−6). (D) Sections of mouse pancreas were analyzed by immunofluorescence using antibodies to insulin (red) and glucagon (green); scale bar, 50 μm (n = 3). (E−G) Hepatic triglyceride levels (E), body weight (F), plasma GLP-1 (G) of mice treated with metformin or FMT (n = 5−6). (H, I) Oil Red O staining on liver tissues; H&E staining of subcutaneous white adipose tissue (sWAT); scale bar, 50 μm (n = 3). (J−L) OGTT and AUC (J), fasting glucose (K) and body weight (L) of *B. pseudocatenulatum*-colonized mouse recipients receiving non-responders' fecal microbiota (n = 5−6). P value determined by two-tailed unpaired Student's t-test, Mann−Whitney U test, Kruskal−Wallis test and one-way ANOVA. ns, non-significant. All data are presented as mean ± SEM or mean ± SD.

nordeoxycholic acid (Nor-DCA), UDCA, CDCA, DCA levels and the ratio of deconjugated BAs to conjugated BAs were significantly higher in the *P. vulgatus* + MET group than in the HK-*P. vulgatus* + MET group (Fig. 3J).

Then, an effective microbiome modulation strategy was established through the oral administration of cefaclor to reverse metformin resistance by inhibiting *P. vulgatus* (Fig. S5D). HFD-fed mice treated with cefaclor + metformin had similar FBG levels to those in the HFD group before metformin treatment (Fig. S5E). After oral gavage with cefaclor for 7 days, the relative abundance of *P. vulgatus* was significantly reduced (Fig. S5F). Unlike the *P. vulgatus* + cefaclor group, the *P. vulgatus* + cefaclor + MET group showed reversal of metformin resistance, as indicated by the expected improvements, including in glucose tolerance, fasting blood glucose levels, body weight, HOMA-IR and TG while treatment with cefaclor alone did not affect these factors in HFD-fed mice (Fig. 3K; Fig. S5G−S5J). Consistent with the above findings, plasma levels of deconjugated BAs were substantially decreased, and the ratio of deconjugated to conjugated BAs was also lower (Fig. 3L; Fig. S5K). Together, these results show that *P. vulgatus* induces metformin non-responsiveness in HFD-fed mice.

The relative hepatic expression of *Fxr*, *Shp*, and *Cyp7b1* and ileal *Tgr5* (G-protein coupled bile acid receptor 1), which are important

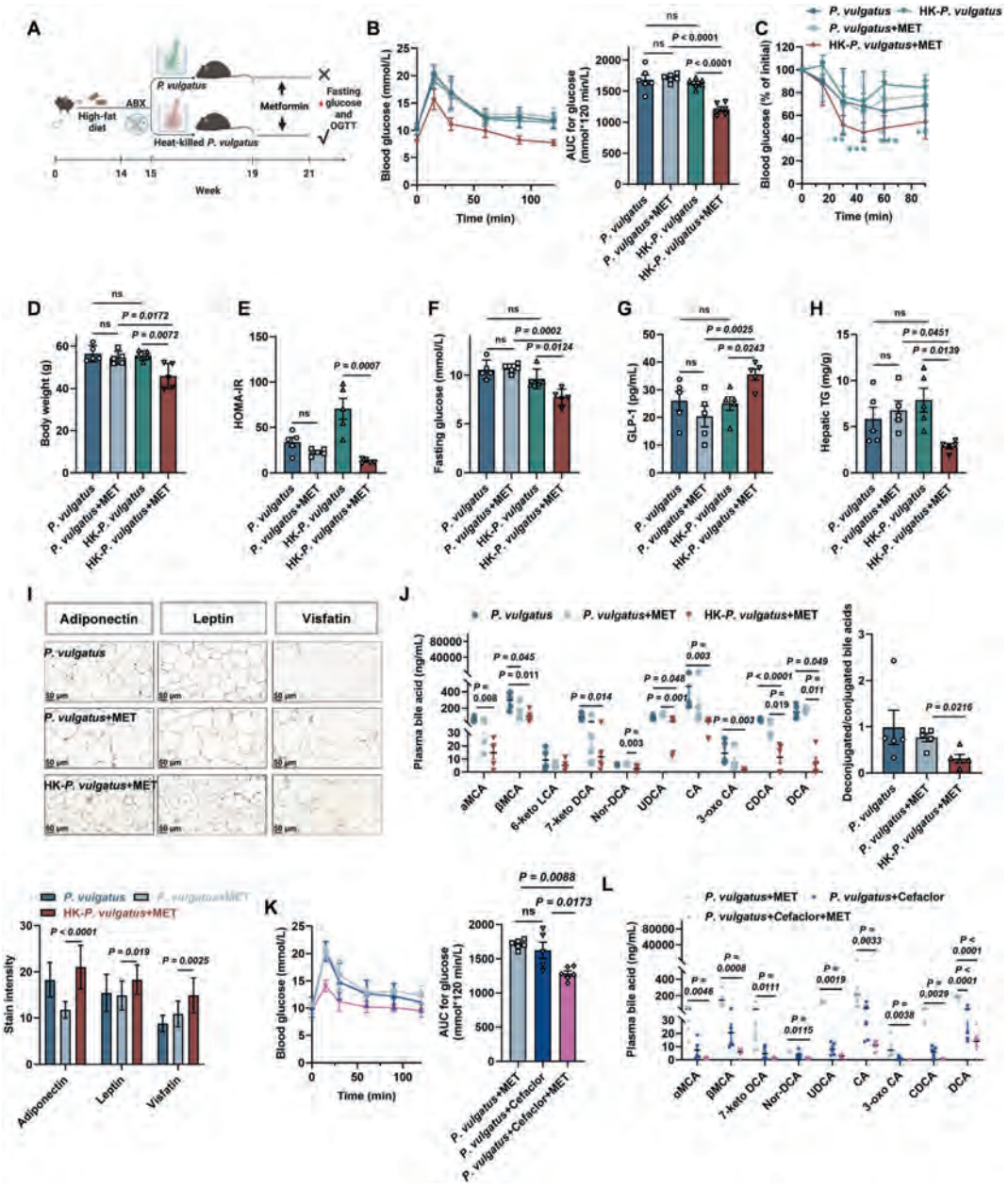

Figure 3 Colonization of *P. vulgatus* reverses the hypoglycemic effect of metformin in HFD-induced mice. Mice were under HFD treatment for 14 weeks to explore the reversal effects. (A) Introduction of *P. vulgatus* strain or HK-*P. vulgatus* in (ABX-induced) microbiota-depleted mice (n = 5−6). (B) OGTT and AUC of *P. vulgatus*-colonized or HK-*P. vulgatus* treated mice (n = 5−6). (C) Insulin tolerance test (ITT) (n = 5). (D−H) body weight (D), HOMA-IR (E), fasting glucose (F), plasma active GLP-1 levels (G) and hepatic triglyceride levels (H) (n = 5−6). (I) adiponectin and leptin immunohistologic staining of sWAT sections; visfatin immunohistologic staining of eWAT sections; scale bar, 50 μm, (five discontinuous sections were evaluated for each sample in three samples per group). (J) Deconjugated bile acid levels in the plasma (n = 5); ratio of deconjugated BAs/conjugated BAs (n = 5). (K) OGTT and AUC of cefaclor treated *P. vulgatus*-colonized mice (n = 5−6). (L) Deconjugated bile acid levels in the plasma (n = 5−6). P value determined by two-tailed unpaired Student's t-test, Mann−Whitney U test, Kruskal−Wallis test and one-way ANOVA. ns, non-significant. All data are presented as mean ± SEM or mean ± SD. αMCA: α-muricholic acid; βMCA: β-muricholic acid.

targets of BAs during metabolism, was downregulated, whereas ileal *Fxr*,*fgf15* (fibroblast growth factor 15) and *Shp* expression was upregulated following *P. vulgatus* colonization (Fig. 4A and B; Fig. S5L and S5M) compared to HK-*P. vulgatus* colonization (Fig. S5N). The mRNA levels of ileal *Ibabp* and *Slc10a2* and hepatic *Hmgcr* (encoding 3-hydroxy-3-methylglutaryl-CoA reductase) were significantly higher in the *P. vulgatus* + MET group, but *Baat* expression did not differ (Fig. S5O−S5Q). Moreover, luciferase reporter assays revealed that CDCA, UDCA, and DCA significantly activated FXR. In addition, both GUDCA and TUDCA markedly repressed GW4064- or CDCA-induced FXR transcriptional activity (Supporting Information Fig. S6A−S6C). Consistently, we found that mice treated with GUDCA + MET or TUDCA + CAPE + MET were responsive to metformin (Fig. 4C

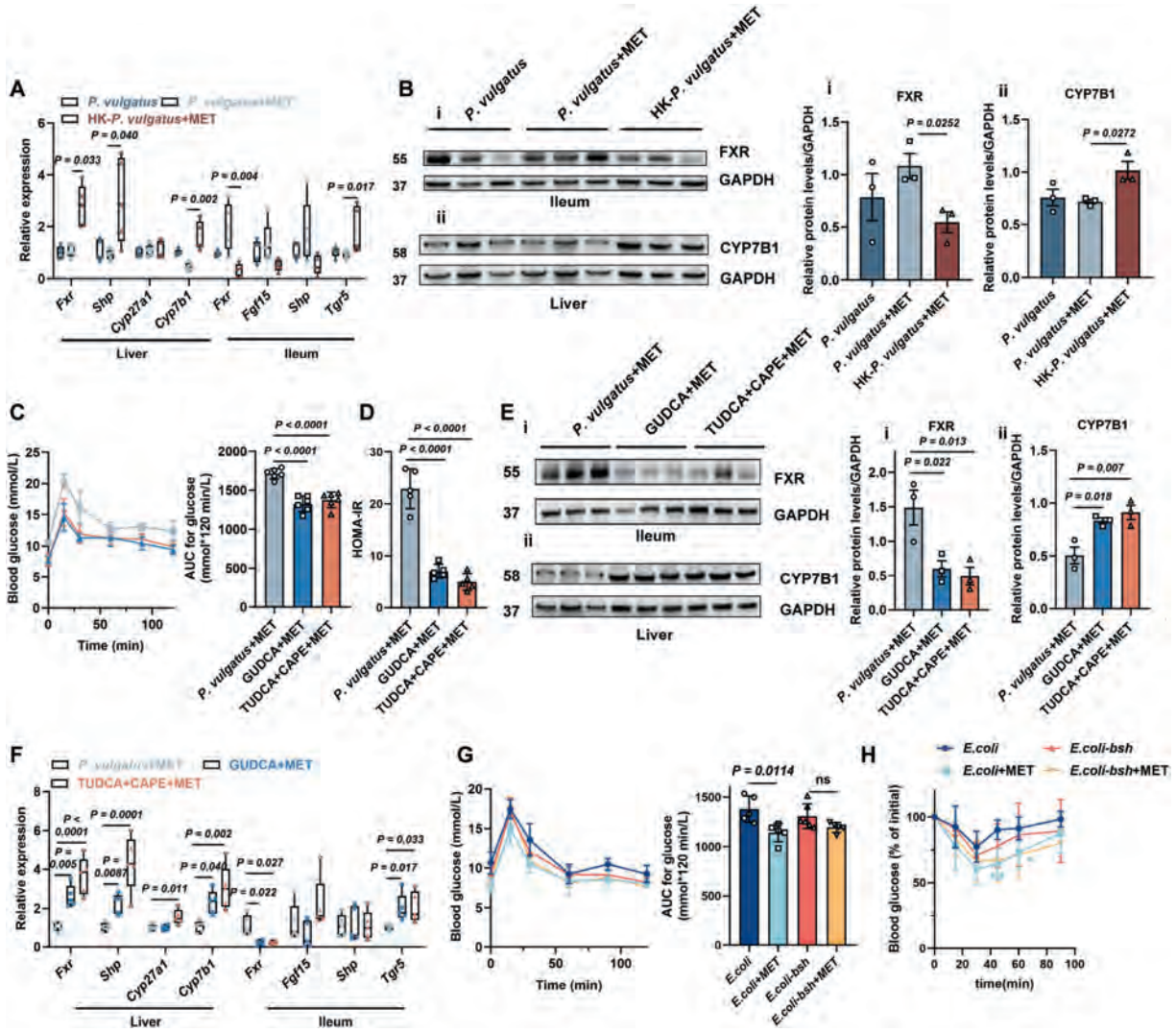

Figure 4 *P. vulgatus*-induced metformin nonresponse involved intestinal FXR signaling, but not exclusively. (A) Relative mRNA abundance of *Fxr*, its target genes, and *Tgr5* mRNAs in the liver and ileum ($n = 5$). (B) Western blot analysis of ileal FXR (i) and hepatic CYP7B1 (ii) protein expression and the statistical graph ($n = 3$). (C, D) OGTT and HOMA-IR of *P. vulgatus*-colonized mice treated with GUDCA or TUDCA + CAPE ($n = 5-6$). (E) Western blot analysis of ileal FXR (i) and hepatic CYP7B1 (ii) protein expression and the statistical graph ($n = 3$). (F) Relative mRNA abundance of *Fxr*, its target genes, and *Tgr5* mRNAs in the liver and ileum ($n = 5$). (G, H) OGTT and ITT of *E. coli*-colonized mice treated with metformin or vehicle control ($n = 5$). *P* value determined by two-tailed unpaired Student's *t*-test, Mann−Whitney U test, Kruskal−Wallis test and one-way ANOVA. ns, non-significant. All data are presented as mean ± SEM or mean ± SD.

and D; Fig. S6D−S6G), even though the relative abundance of *P. vulgatus* was still higher in these mice than before colonization (Fig. S6H). No differences in FBG levels were found among the groups before supplementation (Fig. S6I). Plasma levels of GUDCA and TUDCA were significantly increased after supplementation by gavage (Fig. S6J). Interestingly, the administration of TUDCA or CAPE resulted in no improvement in oral glucose tolerance (Fig. S6K), as TUDCA was rapidly hydrolysed by *P. vulgatus* within 3 h. Intestinal *Fxr* expression was attenuated in the GUDCA + MET and TUDCA + CAPE + MET groups compared with the *P. vulgatus* + MET group. The relative expression of hepatic *Fxr* and *Shp*, ileal *Tgr5* and hepatic CYP7B1 was increased (Fig. 4E and F). Ileal BA absorption was reduced in the GUDCA + MET group due to decreased ileal *Ibabp* and *Slc10a2* mRNA levels (Fig. S6L).

To further verify whether BSH of *P. vulgatus* influences metformin, *BVU_ 2699*, one of the BSH coding genes, was introduced into *Escherichia coli via* LC−MS/MS and electrophoresis validation (Supporting Information Fig. S7A). Surprisingly, despite the strong ability of the knock-in of *BVU_ 2699* and in the *P. vulgatus* culture supernatants to degrade conjugated BAs *in vitro* (Fig. S7B), mice treated with *bsh-knock-in E. coli* showed only a slight reduction in the hypoglycaemic effect of metformin compared with those treated with wild-type (WT) *E. coli via* OGTT and ITT (Fig. S7C and Fig. 4G and H). In addition, to examine the role of FXR activation in MMF, *db/db* mice were subjected to a hyperglycaemia model and received either metformin alone or in combination with CDCA, which is the most potent endogenous FXR agonist[22] or mixture of BAs [LCA, DCA and CA]. However, OGTT revealed that expected metformin-induced improvement in glucose intolerance was not reversed by CDCA or the mixture significantly (Fig. S7D), although the

expression of intestinal *Fxr* and its target genes, but not *Tgr5*, were reversed after CDCA treatment (Fig. S7E).

Collectively, BAs produced by *P. vulgatus* activate FXR in the intestine to reduce the therapeutic effects of metformin. However, there may still be other unknown causes.

3.5. P. vulgatus triggers ceramide-mediated mitochondrial dysfunction to decrease glucose tolerance

To reveal the molecular mechanisms by which *P. vulgatus* affects hepatocyte energy metabolism, we performed RNA-seq analysis of livers from mice treated with metformin or *P. vulgatus* + MET. A total of 822 differentially expressed genes (DEGs) were identified (Fig. 5A); the upregulated DEGs were mostly enriched for ribosomal components, and the downregulated DEGs were enriched for oxidative phosphorylation (OXPHOS), including respiratory electron transport and ATP synthesis, indicating decreased mitochondrial respiratory chain (MRC) activity (Fig. 5B and Supporting Information Fig. S8). Consistently, we detected a higher levels of hepatic reactive oxygen species (ROS) in mice subjected to FMT from nonresponder donors or *P. vulgatus* colonization than in their control groups (Fig. 5C and D). Since dysregulation of mitochondrial function can increase ROS production, we measured the hepatic mitochondrial membrane potential (MMP), which was significantly lower in *P. vulgatus*-colonized mice and could not be improved by metformin

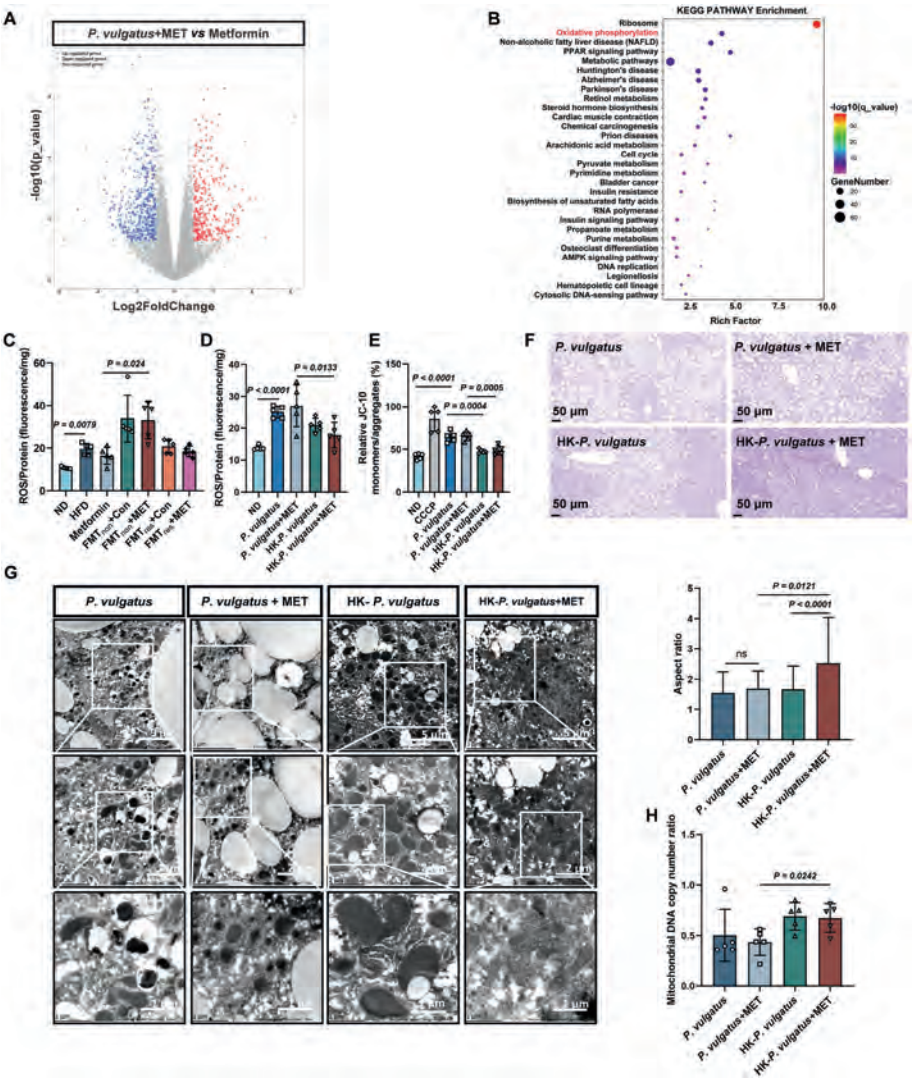

Figure 5 *P. vulgatus* promotes hepatic mitochondrial dysfunction. (A) Volcano plot of significantly upregulated (red), downregulated (blue) genes and non-significant (gray) genes ($n = 3$). (B) KEGG enrichment analysis between *P. vulgatus* + MET *vs* Metformin mice liver samples ($n = 3$). (C) Hepatic ROS levels in mice recipients receiving responders or nonresponders fecal microbiota ($n = 5$). (D) Hepatic ROS levels in *P. vulgatus* or HK-*P. vulgatus* pretreated mice ($n = 5$). (E) Hepatic mitochondrial membrane potential was detected by JC-10 assay, which was measured at Ex/Em = 490/530 nm (monomers) and 525/590 nm (aggregates) ($n = 5$); carbonyl cyanide 3-chlorophenylhydrazone (CCCP) was used as positive controls. (F) PAS staining of liver tissues; scale bar, 50 μm ($n = 3$). (G) Representative transmission EM images of liver sections of *P. vulgatus* and HK-*P. vulgatus* pretreated mice with or without metformin; scale bar, 5000, 2000 and 1000 nm. Mitochondrial aspect ratios were measure by three discontinuous sections. (H) Decreased mitochondrial DNA copy number ($n = 5$). *P* value determined by two-tailed unpaired Student's *t*-test, Mann−Whitney U test, Kruskal−Wallis test and one-way ANOVA. ns, non-significant. All data are presented as mean ± SEM or mean ± SD.

(Fig. 5E). Furthermore, metformin did not increase the periodic acid-Schiff (PAS)-positive area of hepatic cells around the central vein in *P. vulgatus*-enriched mice, indicating impaired glycogen synthesis (Fig. 5F).

Next, we determined the effects of *P. vulgatus* on hepatic mitochondrial morphology *via* transmission electron microscopy (TEM) imaging. Compared with those in HK-*P. vulgatus* + MET pretreated mice, mitochondria in the liver of *P. vulgatus*-colonized mice exhibited a significant reduction in the aspect ratio and count, implying the presence of smaller punctate mitochondria and the potential occurrence of pyknosis (Fig. 5G). Droplet digital PCR (ddPCR) showed that mitochondrial DNA copy number (mtDNA-CN) was also decreased, as assessed by the complex I marker mt−Nd1 (Fig. 5H). There was no significant difference in plasma thioredoxin-interacting protein (TXNIP) levels between the *P. vulgatus* and HK-*P. vulgatus* groups (Supporting Information Fig. S9A). Moreover, insulin levels were obviously elevated in *P. vulgatus* mice (Fig. S9B). Therefore, these results suggest that impaired hepatic mitochondrial morphology and networking and decreased respiratory function ultimately result in severe glucose intolerance, rather than insufficient insulin secretion, in *P. vulgatus*-colonized mice.

In the cohort trial described above, we found that the glycosphingolipid biosynthesis pathway was enriched in the nonresponder group, according to KEGG pathway enrichment analysis of metagenome functional content (Fig. S9C). Glycosphingolipid biosynthesis was a downstream pathway for sphingosine. Interestingly, *Bacteroides* spp. express serine palmitoyltransferase (SPT) to produce bacterial sphingolipids, which can generate ceramides[27]. *P. vulgatus* expresses similar homologous genes, which may produce bacterial sphingolipids that affect host lipid metabolism. Consistently, we observed that metformin treatment resulted in significant upregulation of *BVU_RS04490* and *BVU_RS1*0440 mRNA in *P. vulgatus* (Fig. S9D), which encode aminotransferase class I/II-fold pyridoxal phosphate-dependent enzymes to synthesize sphingolipids.

We conducted a targeted lipidomic analysis of the liver, and C22 ceramide (d18:1/22:0), C24 ceramide (d18:1/24:0), C16:1 ceramide (d18:1/16:1) and C22:1 ceramide (d18:1/22:1) levels were significantly higher in the *P. vulgatus* + MET group than in the HK-*P. vulgatus* + MET group (Fig. 6A). In contrast to the levels in the HK-*P. vulgatus* group (Fig. S9E), the mRNA levels of ceramide synthase genes were significantly increased in the liver and ileum of the *P. vulgatus* + MET group (Fig. 6B). The expression of fatty acid synthesis-related genes, such as those encoding sterol response element-binding protein 1c (*Srebp1c*), were also monitored in the liver and was significantly higher than that in the HK-*P. vulgatus* + MET group (Fig. 6B). HK-*P. vulgatus* mice treated with metformin revealed decreased expression and cleavage-mediated activation of transcription factor SREBP1 compared to control-*P. vulgatus* + MET-treated mice (Fig. 6C). Total ceramide levels were significantly increased in epididymal white adipose tissue (eWAT) after metformin treatment in the *P. vulgatus*-rich group (Fig. 6D). Accordingly, the mRNA level of *Cers6* (ceramide synthase 6) was increased (Fig. 6E). Consistently, the increase in total ceramide levels in eWAT was reversed by FXR inhibitors (Fig. 6F and G). Ileal *Degs1* (delta 4-desaturase, sphingolipid 1), *Sptlc3* (serine palmitoyltransferase long chain base subunit 3), *Smpd3* (sphingomyelin phosphodiesterase 3), and *Cers2* (ceramide synthase 2) expression were also downregulated (Fig. 6H). Myriocine, the SPT inhibitor, potently improved glucose tolerance in *P. vulgatus*-colonized mice (Fig. 6I). All these results suggest that the hepatic FXR−ceramide/SREBP1C/DNA fragmentation factor α-like effector A (CIDEA) pathway was activated in the *P. vulgatus* + MET group. *P. vulgatus* induces MMF by increasing oxidative stress and decreasing OXPHOS in hepatocytes *via* increased ceramide levels.

3.6. C22:0 ceramide exacerbates MFF/Drp1-mediated mitochondrial fragmentation

CerS6-derived sphingolipids interact with Mff to regulate mitochondrial dynamics through Drp1[19]. We therefore measured the affinity of C22:0, C22:1 and C16:0 ceramides bound to human MFF protein by Biacore assay. Interestingly, C22:0 showed the highest affinity among them (Fig. 7A; Fig. S9F). These findings were further verified by MitoTracker red staining. In high-sucrose-challenged liver cells, the MMP of HepG2 cells was significantly decreased after treatment with a high level of ceramide (d18:1/22:0), but treatment with a low level of ceramide increased the MMP. Metformin did not alleviate the decrease in the MMP, which was improved by mitochondrial division inhibitor 1 (mdivi-1) (Fig. 7B). In contrast, the same concentration of ceramide (d18:1/16:0) and ceramide (d18:1/22:1) did not have such a significant effect on MMP (Fig. S9G). CerS6-derived C16:0 sphingolipids are a major contributor to mitochondrial fragmentation in obesity[19]. However, C22:0 ceramide (d18:1/22:0) or C22:1 ceramide (d18:1/22:1) were not reported. To confirm whether ceramide regulates the effects of metformin, we administered ceramide (d18:1/22:0) or ceramide (d18:1/22:1) by intraperitoneal (i.p.) injection. Consistently, the hypoglycaemic effect of metformin was reversed by ceramide (d18:1/22:0) administration (Fig. 7C), but not ceramide (d18:1/22:1) (Fig. S9H). The analysis of mitochondrial morphology by TEM revealed fragmented hepatic mitochondria with a lower aspect ratio in ceramide (d18:1/22:0)-treated mice than in myriocine-treated mice (Fig. S9I). Next, we measured the oxygen consumption rate (OCR) in HepG2 cells. Consistent with the MMP assay results, liver cells treated with a high level of ceramide (d18:1/22:0) showed lower respiration than vehicle-treated cells (Fig. 7D; Fig. S9J). Given the crucial role of Drp1 in the regulation of mitochondrial fission, we investigated whether ceramide (d18:1/22:0) can modulate mitochondrial morphology. Incubation of HepG2 cells with a high level of ceramide (d18:1/22:0) and BSA-conjugated oleic acid/palmitate promoted significant fragmentation of mitochondria, while cells treated with mdivi-1 exhibited reduced mitochondrial fragmentation upon ceramide (d18:1/22:0) challenge (Fig. S9K). Taken together, these results suggest that ceramide (d18:1/22:0) modulates the metabolic demands of high-sucrose-challenged liver cells.

Indeed, vacuolar-type ATPase (v-ATPase) activity, which can be suppressed by metformin[28], affects mitochondrial dynamics by inducing VB12 deficiency to inactivate metr-1[29]. Accordingly, we observed increased mitochondrial fission in the presence of metformin (Supporting Information Fig. S10A). VB12 deficiency and higher homocysteine (Hcy) and methylmalonic acid (MMA) levels were present in the *P. vulgatus* + MET group (Fig. S10B−S10D). Confirming our previous results, adenosylcobalamin supplementation (i.p.) ameliorated the negative impact of *P. vulgatus* on metformin-induced glucose tolerance (Fig. 7E) and improved the hepatic MMP (Fig. 7F). Subsequently, we observed that mdivi-1 significantly improved glucose tolerance and metformin resistance in mice after *P. vulgatus* colonization. Intriguingly, after mdivi-1 withdrawal for 2 weeks, up to 100% of mice

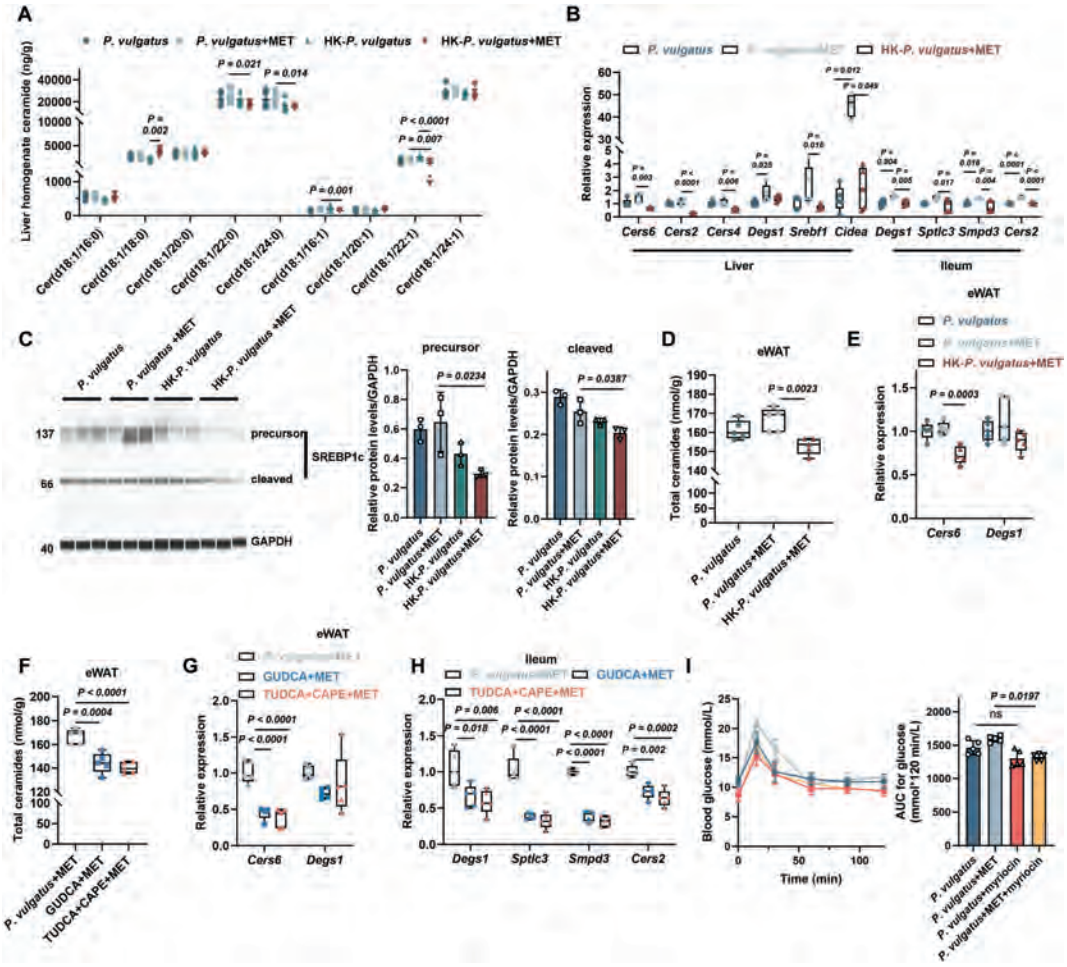

Figure 6 *P. vulgatus* + MET upregulates ceramides biosynthesis to reduce the therapeutic effects of metformin. (A) Quantification of hepatic ceramide (Cer) profiles ($n = 5$). (B) Relative mRNA levels for encoding enzymes involved in ceramides biosynthesis and fatty acid genes in the liver and ileum ($n = 5$). (C) Precursor and mature forms of SREBP1c proteins from hepatic tissue protein detected by capillary blot ($n = 3$). (D−G) Total ceramide levels in eWAT and relative mRNA levels for encoding enzymes involved in ceramides biosynthesis genes in eWAT ($n = 5$). (H) Relative mRNA levels for encoding enzymes involved in ceramides biosynthesis genes in ileum of GUDCA- or TUDCA + CAPE-treated mice ($n = 5-7$). (I) OGTT and AUC of myriocin-treated mice with *P. vulgatus*-colonization ($n = 5$). *P* value determined by two-tailed unpaired Student's *t*-test, Mann−Whitney U test, Kruskal−Wallis test and one-way ANOVA. ns, non-significant. All data are presented as mean ± SEM or mean ± SD.

relapsed to metformin resistance (Fig. 7G; and Fig. S10E and S10F). *P. vulgatus* and *P. vulgatus* + MET mice showed significantly increased hepatic expression of *Mff*, *Drp1*, *Aifm1* (apoptosis inducing factor mitochondria associated 1), *Vdac1* (voltage-dependent anion channel 1) and *Ucp2* (uncoupling protein 2), indicating enhanced mitochondrial fragmentation and apoptosis (Fig. 7H; Fig. S10G and S10H), which could be reversed by GUDCA or TUDCA + CAPE treatment (Fig. 7I). Both total and phosphorylated (serine 616, S616) Drp1 levels were increased by metformin treatment in *P. vulgatus*-colonized mice and ceramide (d18:1/22:0)-treated mice (Fig. 7J; Fig. S10I). Two additional anti-diabetic drugs, dapagliflozin (SGLT2 inhibitor) and pioglitazone (PPARγ agonist), were administered for a period of two weeks to HFD-fed mice in the presence or absence of *P. vulgatus* colonization. Interestingly, OGTT indicated that the effects of pioglitazone were not affected by *P. vulgatus*, whereas those of dapagliflozin were (Supporting Information Fig. S11A and S11B). This may be attributed to pioglitazone-mediated downregulation of *p*-Drp1(Ser616) expression[30], whereas dapagliflozin was found to increase DRP1 protein levels[31]. Collectively, these results indicate that *P. vulgatus* and ceramide (d18:1/22:0) promote hepatic mitochondrial fission after metformin administration.

Following OXPHOS damage, *P. vulgatus*-colonized mice displayed decreased expression of genes associated with mitochondrial respiratory chain complex I, complex III, complex IV and complex V and nicotinamide adenine dinucleotide (NAD) metabolism (Fig. 7K; Fig. S11C); these changes in gene expression were ameliorated by adenosylcobalamin (Fig. S11D). Consistent with the above results, the ability of metformin to improve electron transport chain activity in HFD-fed mice was reversed by ceramide (d18:1/16:0) administration (Fig. S11E). Mitochondrial dysfunction, together with OXPHOS damage and decreased biomolecule synthesis, facilitates the progression to intrahepatic

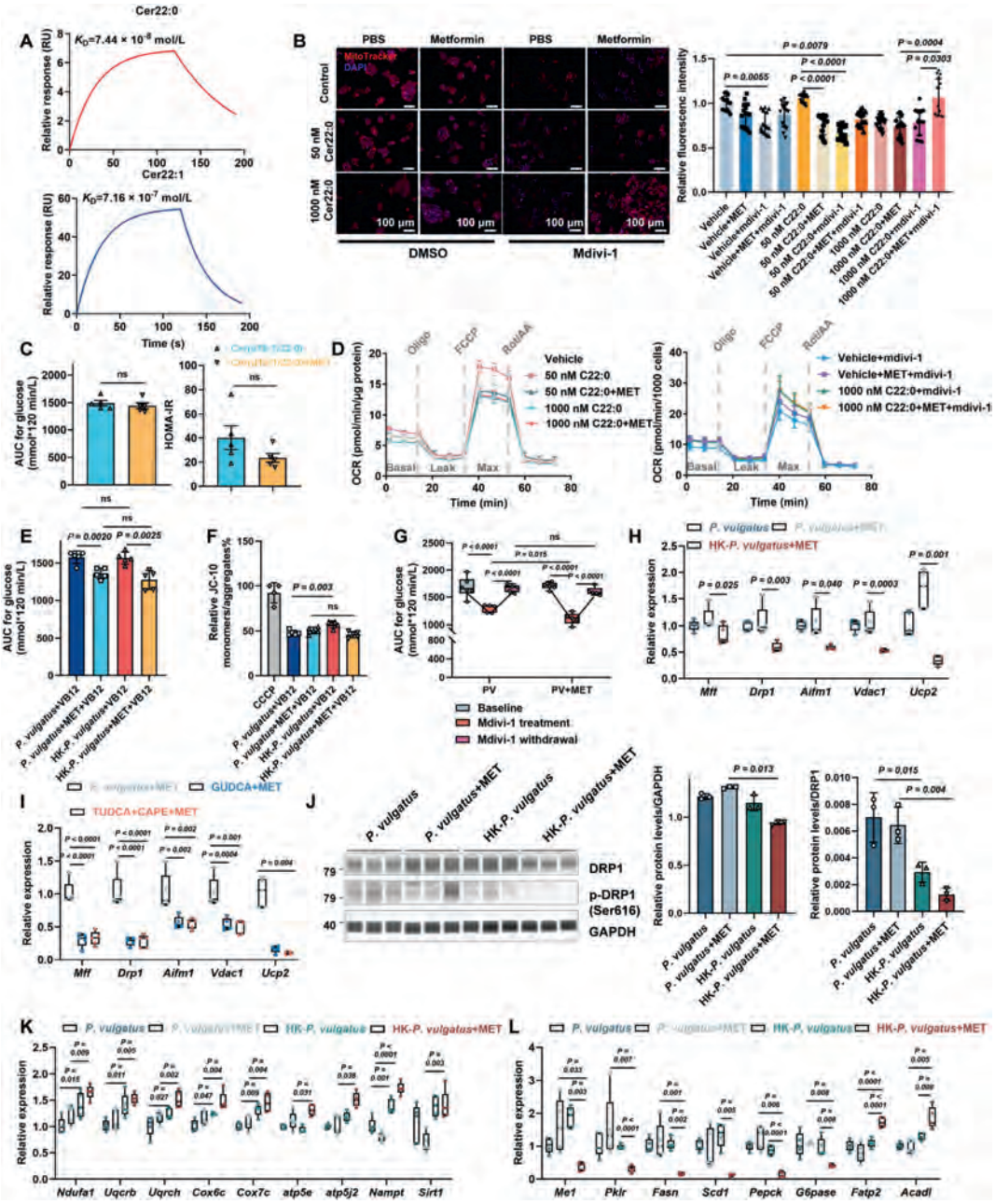

Figure 7 *P. vulgatus* + MET induce mitochondrial fragmentation, OXPHOS damage and fatty acid β-oxidation decrease. (A) The affinity of Cer(d18:1/22:0) and Cer(d18:1/22:1) with human MFF proteins were calculated by SPR. (B) Mitochondrial membrane potential was detected by MitoTracker staining; scale bar: 100 μm. (C) Oral glucose tolerance test AUC and HOMA-IR between Cer(d18:1/22:0) with vehicle or with metformin ($n = 5$). (D) Oxygen consumption rate (OCR) of sucrose-conditioned HepG2 cells ($n = 3$). (E) OGTT of adenosylcobalamin-treated mice with *P. vulgatus*- or HK-*P. vulgatus*-colonization ($n = 5$). (F) Hepatic mitochondrial membrane potential was detected by JC-10 assay ($n = 5$). (G) Oral glucose tolerance test AUC ($n = 5$−6); HFD-mice that received *P. vulgatus* before drug treatment were classified as baseline; mice treated with metformin (200 mg/kg) and mdivi-1 (1.2 mg/kg) for 2 weeks were classified as mdivi-1 treatment; mice continued metformin treatment but mdivi-1 withdrawal for 2 weeks as mdivi-1 withdrawal. (H, I) Relative mRNA expression of *Mff*, *Drp1*, *Aifm1*, *Vsac1* and *Ucp2* in liver ($n = 5$). (J) The expression of DRP1, *p*-DRP1(Ser616) and GAPDH in hepatic tissue protein ($n = 3$). (K) mRNA levels of mitochondrial respiratory chain genes (*Ndufa1*, *Uqcrb*, *Uqcrh*, *Cox6c*, *Cox7c*, *Atp5e* and *Atp5j2*) and NAD metabolism (*Nampt* and *Sirt1*) genes in liver ($n = 5$). (L) mRNA levels of fatty acid synthesis (*Me1*, *Pklr*, *Fasn* and *Scd1*), gluconeogenesis (*Pepck* and *G6pase*) and fatty acid oxidation (*Fatp2* and *Acadl*) genes in liver ($n = 5$). *P* value determined by two-tailed unpaired Student's *t*-test, Mann−Whitney U test, Kruskal−Wallis test and one-way ANOVA. ns, non-significant. All data are presented as mean ± SEM or mean ± SD. M, mol/L.

lipid accumulation, gluconeogenesis, and reduced hepatic fatty acid β-oxidation and glycogen synthesis. Next, we measured the relative expression of genes related to fatty acid synthesis, gluconeogenesis and fatty acid oxidation in the liver; the data show significant increases in expression, resulting in systemic insulin resistance and hepatic lipid accumulation (Fig. 7L). Interestingly, metformin treatment led to improvements in HFD or HK-*P. vulgatus* mice, but *P. vulgatus* mice showed complete loss of benefit from metformin or even exhibited aggravation of these responses.

Mitochondria are powerful generators of heat. Adipose tissue thermogenesis is related to improved obesity and systemic glucose homeostasis due to increased adaptive thermogenesis and energy expenditure. Brown adipose tissue (BAT) thermogenesis consumes excess energy to improve glycaemic control and blood lipid levels by utilizing blood sugar and fatty acids in mitochondria, which is directly related to metabolic diseases, such as obesity, diabetes, and fatty liver[32]. Damaged mitochondria cannot support efficient thermogenesis. *Ucp1* (uncoupling Protein 1), *Elovl3* (ELOVL fatty acid elongase 3), *Ckmt2* (creatine kinase, mitochondrial 2), and *PPAR-*γ (peroxisome proliferator-activated receptor γ), as the key genes in BAT, mediate energy dissipation to heat, BAT recruitment, energy transduction, and brown adipocyte differentiation, processes that can be regulated by adipose FXR, TGR5, and ceramide levels. To further determine whether thermogenesis is altered by metformin in *P. vulgatus*-colonized mice, we evaluated several thermogenesis indicators. In *P. vulgatus* + MET mice, we observed inhibition of thermogenesis-related gene expression (Fig. S11F and S11G). Consistent with previous results, GUDCA + MET and TUDCA + CAPE + MET reversed the changes in *Fxr* and *Tgr5* gene expression and thermogenic gene expression in eWAT and BAT (Fig. S11H and S11I).

To reiterate the interrelationship between FXR−DRP1−lipid accumulation and thermogenic damage, glycine-β-muricholic acid (Gly-β-MCA), an intestinal FXR-specific inhibitor that has been proven ineffective in intestine-specific *Fxr*-null mice[18], was validated. Consistently, Gly-β-MCA could restore the efficacy of metformin in mice colonized with *P. vulgatus* (Supporting Information Fig. S12A) by suppressing intestinal FXR (Fig. S12B). Hepatic CYP7B1 was upregulated by Gly-β-MCA (Fig. S12C), and lipid accumulation was concomitantly decreased (Fig. S12D). Subsequently, DRP1 levels were decreased (Fig. S12E) and thermogenic gene expression promoted (Fig. S12F).

To investigate the direct impact of *P. vulgatus* on mitochondrial injury, a treatment regimen involving cefaclor was administered to *P. vulgatus* mice, which demonstrated a notable reduction in the expression of hepatic MFF and DRP1 in comparison to the control group (Fig. S12G and S12H). Additionally, cefaclor was found to induce a recuperated expression of genes linked to the mitochondrial respiratory chain and NAD metabolism, while concurrently reducing the expression of genes associated with fatty acid synthesis, gluconeogenesis, and enhancing fatty acid oxidation (Fig. S12I and S12J). It was thus demonstrated that the suppression of *P. vulgatus* growth with cefaclor represented an improvement with respect to the mitochondrial damage induced by *P. vulgatus*.

These changes suggest that *P. vulgatus* could activate the FXR−ceramide axis to induce DRP1-dependent hepatic mitochondrial fission, lipid accumulation and damage to adipose thermogenesis, which could be reversed by VB12, mdivi-1 and cefaclor.

4. Discussion

Nonresponsiveness to metformin limits its use in clinical practice. The heritability of metformin response, based on common variants captured by classical genotyping arrays, ranges from only 20%−34% (moderately heritable)[33]. Therefore, pharmacogenetics cannot explain the discrepancies in MMF, suggesting that environmental factors, such as symbiotic microbiota, are another key determinant of this phenomenon. Approximately 30% of administered metformin remains unmetabolized in faeces, which leads to noticeable effects on the gut microbiome[34]. However, the biotransformation or bioaccumulation of metformin by human gut microbes has not yet been observed. Moreover, for metformin, dosage analysis is associated with microbiome shifts towards the *Bacteroides* 2 enterotype, which is proposed to be a severity marker in T2DM[35]. Thus, it is unclear whether the regulation of the gut flora by metformin is necessarily beneficial.

Based on metagenomic analysis, *Bifidobacterium* spp., *Veillonella* spp. and *Streptococcus* spp. were enriched in responders before metformin treatment, while *Ruminococcus* spp. and *Alistipes spp*. in nonresponders before metformin. After 3 months of oral metformin, we found an accumulation of *Bacteroides* spp. and *Phocaeicoia spp.* in MMF patients. *In vitro*, metformin promoted *Sutterella wadsworthensis*, while it suppresses *Clostridium difficile* and *Fusobacterium nucleatum* growth. These findings may explain why metformin treatment seems to have a protective effect against the development of *C. difficile* infection[36] or to overcome chemoresistance in colorectal cancer caused by *F. nucleatum*[37]. However, the growth curve of *P. vulgatus* showed a mildly higher maximum growth concentration, indicating that the increase in *P. vulgatus* in nonresponders may be due to complex host−microbiota interactions rather than to the effects of metformin alone. It was reported that metformin could inhibit the rate of bacterial growth of *E. coli* by disturbing bacterial folate and methionine metabolism *in vitro*[38]. We have tried to analyse the transcriptional responses of *P. vulgatus* culture. Metformin had little significant influence but increased its capacity to withstand environmental stress. This could potentially facilitate the proliferation of *P. vulgatus* in nutrient-deprived environments, particularly in the context of glucose limitation. Interestingly, the expression of functional β-galactosidase was higher in the nonresponder faecal samples, which could breakdown lactose into its two monosaccharide components to produce lactate. Lactate enhances polysaccharide utilization and promotes the growth of *P. vulgatus*[25], which may also account for its enrichment in the nonresponder group.

In this study, we identified *P. vulgatus* as a mediator that reduced the therapeutic effects of metformin through regulation of BA metabolism with strong BSH activity. Increased abundance of *P. vulgatus* was positively correlated with the ratio of deconjugated/conjugated BAs. Considering that the bile acid-FXR−FGF15 signalling pathway is a well-clarified pathway[39,40], we firstly hypothesized that *P. vulgatus* can activate the intestinal Fxr−Fgf15 signalling pathway and suppress the hepatic Fxr−Shp axis to induce a stable metformin resistance model involving the gut microbiota. These impaired effects could be reversed by the administration of intestinal FXR inhibitors (GUDCA or TUDCA). Interestingly, probiotics of BSH-producing *Bifidobacterium* may lose their protective effect against T2DM.

However, BSH-knockin *E. coli* showed slightly impaired metformin effects *via* OGTT and ITT, prompting us to investigate further. We observed that ileal and hepatic ceramide biosynthesis genes were prominently upregulated in *P. vulgatus*-colonized mice

after metformin treatment. Hepatic Srebf1 and *Cidea* gene expression was also significantly upregulated in the *P. vulgatus* + MET group, suggesting that de novo fat production increased to promote hepatic triglyceride accumulation. The activation of FXR could increase sphingomyelin phosphodiesterase 3 (SMPD3)-induced ceramide levels[41]. Moreover, the FXR−ceramide/SREBP1C/CIDEA pathway could respond to hepatic triglyceride accumulation[42]. Recent studies have shown that the activation of intestinal FXR signalling enhances the synthesis of ceramides to promote metabolic disease, which in turn significantly affects HOMA-IR[43,44]. Specially, ceramide C22:0 has been reported to play a role in the aetiology of T2D, supported by genome-wide association studies and Mendelian randomization analyses[45]. Our study employed four "function blockades" (VB12, myriocin, mitochondrial division inhibitor 1 [mdivi-1] and antioxidant [TUDCA]) and two "function strengthening" perturbations (*B. pseudocatenulatum* and Cer (d18:1/22:0)); the data were fully consistent across all six treatments. We noticed that under metformin treatment, *P. vulgatus* colonization resulted in a higher level of ceramides, which play a critical role in mitochondrial dysfunction.

T2DM involves mitochondrial dysfunction in the liver, muscle and adipose tissue, which are all organs with high metabolic rates, thus promoting the development of systemic insulin resistance[46]. We observed decreased VB12 levels in the *P. vulgatus* + MET group, indicating increased mitochondrial fission. Compared with HK-*P. vulgatus*-pretreated mice, *P. vulgatus*-pretreated mice exhibited decreased mitochondrial abundance, oxidative capacity damage, increased ROS levels, disturbed respiratory chain function, impaired ATP production and mitochondrial proliferation through fission and fusion due to active BSH and activated intestinal FXR. Interestingly, both our results and those of previous studies have shown that BAs and ceramides can modulate mitochondrial structure, as can metformin, suggesting that they play both overlapping and unique roles. The standard mitochondrial shape depends on the balance between fission and fusion, which mediated by mitochondrial fission/fusion proteins (*i.e.*, Drp1, Fis1 (fission, mitochondrial 1), OPA1 (OPA1, mitochondrial dynamin like GTPase) and Mfn1/2 (mitofusin 1/2)). However, an imbalance in mitochondrial fission−fusion, caused by abnormal Drp1 activation, results in mitochondrial fragmentation, which contributes to mitochondrial and cell dysfunction. And MFF is an essential factor for mitochondrial recruitment of Drp1[47]. Recently, CerS6-derived sphingolipids were demonstrated to interact with Mff to promote mitochondrial fragmentation, which is governed by the phosphorylation of Mff at S155/172 and Drp1 at S616[48]. Supra-pharmacological concentrations of metformin reduce mitochondrial respiration by inhibiting complex I[49], but pharmacological concentrations of metformin activate AMPK by phosphorylation at T172 to promote mitochondrial fission and improve mitochondrial respiration[48]. In addition, metformin inhibits the activity of V-ATPase *via* the PEN2 (presenilin enhancer protein 2)−ATP6AP1 (V-type proton ATPase subunit S1) axis[28]. V-ATPase has a crucial function in lysosomal acidification, which in turn activates acid proteases, enzymes that are essential for degrading intrinsic factor and then releasing VB12 into the cytoplasm. V-ATPase dysfunction-induced mitochondrial biogenesis is mediated by VB12 deficiency[29]. Therefore, the combined effect has disrupted the fission−fusion balance to exacerbate mitochondrial damage caused by excessive fission, thereby further inhibiting mitochondrial respiration in *P. vulgatus*-colonized mice. Indeed, we observed that *Ucp2* expression was significantly higher in mice treated with both *P. vulgatus* and metformin than in those treated with *P. vulgatus* alone. These results are consistent with clinical observations of patients during metformin therapy, indicating that some T2DM patients experience secondary resistance to metformin. Thus, VB12 supplementation-mediated improvement in mitochondrial function offers a promising and safe preventive approach to MMF. Extensive clinical trials are required to further verify the pharmacological effects of VB12 on MMF.

The large individual differences in gut microbiota have led us to rethink the suitability of metformin, particularly in anti-ageing, due to impaired mitochondrial function in the brain resulting in an increased risk of Alzheimer's disease and Parkinson's disease[50]. Our findings emphasize the metformin-induced alteration of *P. vulgatus* in T2DM patients, leading to increased metformin toxicity to mitochondria and reduced glycaemic control. Given the possibility of modulating the gut microbiota to some extent, therapeutic targeting of the microbiome is a promising strategy for improving drug efficacy and safety. Accordingly, it is possible that gut microbial intervention may contribute to the benefits of metformin. There are currently several effective approaches — such as the use of dietary fibre supplements, FMT and bacteriophages — for intentionally manipulating the microbial composition. Herein, we modulated the intestinal microbiota directly with cefaclor, an antibiotic that is often used to treat infections of the respiratory tract and urinary system in the clinic, as it significantly inhibits the growth of *P. vulgatus* but not of other common *Bacteroides* (such as *B. fragilis*, *B. uniformis* and *B. ovatus*)[51]. Consistent with our expectations, cefaclor therapy reversed *P. vulgatus*-induced metformin resistance. Thus, due to gut microbiota−drug crosstalk, drug combinations such as metformin plus a gut microbiota modulator may be another promising strategy and constitute a precision medicine approach for preventing or reversing metformin resistance and for future personalized medicine.

5. Conclusions

In this study, we show significant alterations in the gut microbiota (at both the compositional and functional potential levels) in individuals with metformin nonresponders and responders, which could be transferred to HFD-fed mice through microbiota transplantation from nonresponder donors. Importantly, we also show that worse outcomes of metformin treatment may correlate with an increased abundance of *P. vulgatus* in T2DM patients. This is due not only to the failure of metformin to regulate glucose metabolism in response to BAs/ceramides metabolism mediated by *P. vulgatus* but also to the mitochondrial dysfunction aggravated by the metformin-mediated promotion of mitochondrial fission. The inhibition of hepatic cholesterol catabolism, promotion of ileal ceramide biosynthesis, suppression of adipose thermogenesis and mitochondrial dysfunction ultimately negatively impact the ability of metformin to treat metabolic diseases. Therefore, key approaches for the treatment of MMF could include the suppression of *P. vulgatus* accumulation, inhibition of overactivated ceramides synthesis signalling or improvement in mitochondrial function.

Data availability

Raw metagenomic sequences (No. PRJNA806510, https://dataview.ncbi.nlm.nih.gov/object/PRJNA806510?reviewer=15v7l08q9bgquhddv6b9bk799b) have been deposited at Sequence

Read Archive and are publicly available as of the date of publication. All other data needed to evaluate the conclusions in the paper are available from the corresponding author on reasonable request.

Acknowledgments

This work was supported by the National Key Research and Development Program of China (Nos. 2021YFA1301200), the National Natural Science Foundation of China (Nos. 82073945, 82404770, 82074000 and 81874329), the Postdoctoral Fellowship Program of CPSF (No. GZC20233198, China), the Postgraduate Scientific Research Innovation Project of Hunan Province (No. CX20200121, China), the Fundamental Research Funds for Central Universities of Central South University (No. 2020zzts252, China), Project Program of National Clinical Research Center for Geriatric Disorders (Xiangya Hospital, Grant No. 2020LNJJ06, China), the scientific research project of Furong laboratory of Central South University (No. 2023SK2083, China), and the Hunan Provincial Natural Science Foundation of China (No. 2024JJ5585). The authors thank the participants (Rong Liu, Nian Yang, Mengyu Wang, and Jiahui Cai) for their kind assistance and cooperation in the study, and the High Performance Computing Center of Central South University for partial support of this work.

Author contributions

Manyun Chen: Writing − review & editing, Writing − original draft, Visualization, Validation, Software, Project administration, Methodology, Investigation, Funding acquisition, Formal analysis, Data curation. Yilei Peng: Methodology, Investigation. Yuhui Hu: Methodology, Investigation. Zhiqiang Kang: Resources, Project administration. Ting Chen: Methodology, Investigation. Yulong Zhang: Methodology, Investigation. Xiaoping Chen: Writing − review & editing. Qing Li: Writing − review & editing. Zuyi Yuan: Writing − review & editing. Yue Wu: Writing − review & editing. Heng Xu: Writing − review & editing. Gan Zhou: Project administration. Tao Liu: Resources, Project administration. Honghao Zhou: Writing − review & editing. Chunsu Yuan: Writing − review & editing. Weihua Huang: Supervision, Funding acquisition, Conceptualization. Wei Zhang: Supervision, Funding acquisition, Conceptualization.

Conflicts of interest

The authors declare no conflicts of interest.

Appendix A. Supporting information

Supporting information to this article can be found online at https://doi.org/10.1016/j.apsb.2025.02.008.

References

1. Doyle Delgado K, Chamberlain JJ, Shubrook JH. Pharmacologic approaches to glycemic treatment of type 2 diabetes: synopsis of the 2020 American diabetes association's standards of medical Care in diabetes clinical guideline. *Ann Intern Med* 2020;**173**:813−21.
2. Brown JB, Conner C, Nichols GA. Secondary failure of metformin monotherapy in clinical practice. *Diabetes Care* 2010;**33**:501−6.
3. Palmer SC, Mavridis D, Nicolucci A, Johnson DW, Tonelli M, Craig JC, et al. Comparison of clinical outcomes and adverse events associated with glucose-lowering drugs in patients with type 2 diabetes: a meta-analysis. *JAMA* 2016;**316**:313−24.
4. Pawlyk AC, Giacomini KM, McKeon C, Shuldiner AR, Florez JC. Metformin pharmacogenomics: current status and future directions. *Diabetes* 2014;**63**:2590−9.
5. Dujic T, Zhou K, Yee SW, van Leeuwen N, de Keyser CE, Javorský M, et al. Variants in pharmacokinetic transporters and glycemic response to metformin: a metgen meta-analysis. *Clin Pharmacol Ther* 2017;**101**:763−72.
6. Zhou K, Bellenguez C, Spencer CC, Bennett AJ, Coleman RL, Tavendale R, et al. Common variants near ATM are associated with glycemic response to metformin in type 2 diabetes. *Nat Genet* 2011;**43**:117−20.
7. Zhou K, Yee SW, Seiser EL, van Leeuwen N, Tavendale R, Bennett AJ, et al. Variation in the glucose transporter gene SLC2A2 is associated with glycemic response to metformin. *Nat Genet* 2016;**48**:1055−9.
8. Forslund K, Hildebrand F, Nielsen T, Falony G, Le Chatelier E, Sunagawa S, et al. Disentangling type 2 diabetes and metformin treatment signatures in the human gut microbiota. *Nature* 2015;**528**:262−6.
9. Wu H, Esteve E, Tremaroli V, Khan MT, Caesar R, Mannerås Holm L, et al. Metformin alters the gut microbiome of individuals with treatment-naive type 2 diabetes, contributing to the therapeutic effects of the drug. *Nat Med* 2017;**23**:850−8.
10. Sun L, Xie C, Wang G, Wu Y, Wu Q, Wang X, et al. Gut microbiota and intestinal FXR mediate the clinical benefits of metformin. *Nat Med* 2018;**24**:1919−29.
11. Zhu X, Shen J, Feng S, Huang C, Wang H, Huo F, et al. *Akkermansia muciniphila*, which is enriched in the gut microbiota by metformin, improves cognitive function in aged mice by reducing the proinflammatory cytokine interleukin-6. *Microbiome* 2023;**11**:120.
12. Christiansen CB, Gabe MBN, Svendsen B, Dragsted LO, Rosenkilde MM, Holst JJ. The impact of short-chain fatty acids on GLP-1 and PYY secretion from the isolated perfused rat colon. *Am J Physiol Gastrointest Liver Physiol* 2018;**315**:G53−65.
13. Koh A, Mannerås Holm L, Yunn NO, Nilsson PM, Ryu SH, Molinaro A, et al. Microbial imidazole propionate affects responses to metformin through p38γ-dependent inhibitory AMPK phosphorylation. *Cell Metab* 2020;**32**:643−53.e644.
14. Foretz M, Hébrard S, Leclerc J, Zarrinpashneh E, Soty M, Mithieux G, et al. Metformin inhibits hepatic gluconeogenesis in mice independently of the LKB1/AMPK pathway *via* a decrease in hepatic energy state. *J Clin Investig* 2010;**120**:2355−69.
15. Sun L, Cai J, Gonzalez FJ. The role of farnesoid X receptor in metabolic diseases, and gastrointestinal and liver cancer. *Nat Rev Gastroenterol Hepatol* 2021;**18**:335−47.
16. Watanabe M, Houten SM, Wang L, Moschetta A, Mangelsdorf DJ, Heyman RA, et al. Bile acids lower triglyceride levels *via* a pathway involving FXR, SHP, and SREBP-1c. *J Clin Investig* 2004;**113**:1408−18.
17. Xu S, Jia P, Fang Y, Jin J, Sun Z, Zhou W, et al. Nuclear farnesoid X receptor attenuates acute kidney injury through fatty acid oxidation. *Kidney Int* 2022;**101**:987−1002.
18. Jiang C, Xie C, Lv Y, Li J, Krausz KW, Shi J, et al. Intestine-selective farnesoid X receptor inhibition improves obesity-related metabolic dysfunction. *Nat Commun* 2015;**6**:10166.
19. Hammerschmidt P, Ostkotte D, Nolte H, Gerl MJ, Jais A, Brunner HL, et al. CerS6-derived sphingolipids interact with mff and promote mitochondrial fragmentation in obesity. *Cell* 2019;**177**:1536−52.e1523.
20. Ma H, Guo X, Cui S, Wu Y, Zhang Y, Shen X, et al. Dephosphorylation of AMP-activated protein kinase exacerbates ischemia/reperfusion-induced acute kidney injury *via* mitochondrial dysfunction. *Kidney Int* 2022;**101**:315−30.

21. Wahlström A, Sayin SI, Marschall HU, Bäckhed F. Intestinal crosstalk between bile acids and microbiota and its impact on host metabolism. *Cell Metab* 2016;**24**:41−50.
22. de Aguiar Vallim TQ, Tarling EJ, Edwards PA. Pleiotropic roles of bile acids in metabolism. *Cell Metab* 2013;**17**:657−69.
23. Plovier H, Everard A, Druart C, Depommier C, Van Hul M, Geurts L, et al. A purified membrane protein from *Akkermansia muciniphila* or the pasteurized bacterium improves metabolism in obese and diabetic mice. *Nat Med* 2017;**23**:107−13.
24. Shih CT, Yeh YT, Lin CC, Yang LY, Chiang CP. *Akkermansia muciniphila* is negatively correlated with hemoglobin A1c in refractory diabetes. *Microorganisms* 2020;**8**:1360.
25. Wu Q, Liang X, Wang K, Lin J, Wang X, Wang P, et al. Intestinal hypoxia-inducible factor 2α regulates lactate levels to shape the gut microbiome and alter thermogenesis. *Cell Metab* 2021;**33**: 1988−2003.e1987.
26. Zhao L, Zhang F. Gut bacteria selectively promoted by dietary fibers alleviate type 2 diabetes. *Science* 2018;**359**:1151−6.
27. Johnson EL, Heaver SL, Waters JL, Kim BI, Bretin A, Goodman AL. Sphingolipids produced by gut bacteria enter host metabolic pathways impacting ceramide levels. *Nat Commun* 2020;**11**:2471.
28. Ma T, Tian X, Zhang B, Li M, Wang Y, Yang C, et al. Low-dose metformin targets the lysosomal AMPK pathway through PEN2. *Nature* 2022;**603**:159−65.
29. Wei W, Ruvkun G. Lysosomal activity regulates *Caenorhabditis elegans* mitochondrial dynamics through vitamin B12 metabolism. *Proc Natl Acad Sci U S A* 2020;**117**:19970−81.
30. Chuang YC, Lin TK, Yang DI, Yang JL, Liou CW, Chen SD. Peroxisome proliferator-activated receptor-gamma dependent pathway reduces the phosphorylation of dynamin-related protein 1 and ameliorates hippocampal injury induced by global ischemia in rats. *J Biomed Sci* 2016;**23**:44.
31. Zhang L, Lin H, Yang X, Shi J, Sheng X, Wang L, et al. Effects of dapagliflozin monotherapy and combined aerobic exercise on skeletal muscle mitochondrial quality control and insulin resistance in type 2 diabetes mellitus rats. *Biomed Pharmacother* 2023;**169**:115852.
32. Sponton CH, Hosono T, Taura J, Jedrychowski MP, Yoneshiro T, Wang Q, et al. The regulation of glucose and lipid homeostasis *via* PLTP as a mediator of BAT-liver communication. *EMBO Rep* 2020; **21**:e49828.
33. Zhou K, Donnelly L, Yang J, Li M, Deshmukh H, Van Zuydam N, et al. Heritability of variation in glycaemic response to metformin: a genome-wide complex trait analysis. *Lancet Diabetes Endocrinol* 2014;**2**:481−7.
34. McCreight LJ, Bailey CJ, Pearson ER. Metformin and the gastrointestinal tract. *Diabetologia* 2016;**59**:426−35.
35. Forslund SK, Chakaroun R, Zimmermann Kogadeeva M, Markó L, Aron Wisnewsky J, Nielsen T, et al. Combinatorial, additive and dose-dependent drug-microbiome associations. *Nature* 2021;**600**:500−5.
36. Eliakim Raz N, Fishman G, Yahav D, Goldberg E, Stein GY, Zvi HB, et al. Predicting *Clostridium difficile* infection in diabetic patients and the effect of metformin therapy: a retrospective, case-control study. *Eur J Clin Microbiol Infect Dis* 2015;**34**:1201−5.
37. Huang X, Hong X, Wang J, Sun T, Yu T, Yu Y, et al. Metformin elicits antitumour effect by modulation of the gut microbiota and rescues *Fusobacterium nucleatum*-induced colorectal tumourigenesis. *EBioMedicine* 2020;**61**:103037.
38. Cabreiro F, Au C, Leung KY, Vergara Irigaray N, Cochemé HM, Noori T, et al. Metformin retards aging in *C. elegans* by altering microbial folate and methionine metabolism. *Cell* 2013;**153**:228−39.
39. Katafuchi T, Makishima M. Molecular basis of bile acid−FXR−FGF15/19 signaling axis. *Int J Mol Sci* 2022;**23**:6046.
40. Guan B, Tong J, Hao H, Yang Z, Chen K, Xu H, et al. Bile acid coordinates microbiota homeostasis and systemic immunometabolism in cardiometabolic diseases. *Acta Pharm Sin B* 2022;**12**:2129−49.
41. Wu Q, Sun L, Hu X, Wang X, Xu F, Chen B, et al. Suppressing the intestinal farnesoid X receptor/sphingomyelin phosphodiesterase 3 axis decreases atherosclerosis. *J Clin Investig* 2021;**131**:e142865.
42. Jiang C, Xie C, Li F, Zhang L, Nichols RG, Krausz KW, et al. Intestinal farnesoid X receptor signaling promotes nonalcoholic fatty liver disease. *J Clin Investig* 2015;**125**:386−402.
43. Apostolopoulou M, Gordillo R, Koliaki C, Gancheva S, Jelenik T. Specific hepatic sphingolipids relate to insulin resistance, oxidative stress, and inflammation in nonalcoholic steatohepatitis. *Diabetes Care* 2018;**41**:1235−43.
44. Lemaitre RN, Yu C, Hoofnagle A, Hari N, Jensen PN, Fretts AM, et al. Circulating sphingolipids, insulin, HOMA-IR, and HOMA-B: the strong heart family study. *Diabetes* 2018;**67**:1663−72.
45. Wittenbecher C, Cuadrat R, Johnston L, Eichelmann F, Jäger S, Kuxhaus O, et al. Dihydroceramide- and ceramide-profiling provides insights into human cardiometabolic disease etiology. *Nat Commun* 2022;**13**:936.
46. Li Z, Gurung M, Rodrigues RR, Padiadpu J, Newman NK, Manes NP, et al. Microbiota and adipocyte mitochondrial damage in type 2 diabetes are linked by *Mmp12*$^{+}$ macrophages. *J Exp Med* 2022;**219**: e20220017.
47. Lacombe A, Scorrano L. The interplay between mitochondrial dynamics and autophagy: from a key homeostatic mechanism to a driver of pathology. *Semin Cell Dev Biol* 2024;**161**−**162**:1−19.
48. Wang Y, An H, Liu T, Qin C, Sesaki H, Guo S, et al. Metformin improves mitochondrial respiratory activity through activation of AMPK. *Cell Rep* 2019;**29**:1511−23.e1515.
49. El Mir MY, Nogueira V, Fontaine E, Avéret N, Rigoulet M, Leverve X. Dimethylbiguanide inhibits cell respiration *via* an indirect effect targeted on the respiratory chain complex I. *J Biol Chem* 2000;**275**: 223−8.
50. Wang W, Zhao F, Ma X, Perry G, Zhu X. Mitochondria dysfunction in the pathogenesis of Alzheimer's disease: recent advances. *Mol Neurodegener* 2020;**15**:30.
51. Maier L, Pruteanu M, Kuhn M, Zeller G, Telzerow A, Anderson EE, et al. Extensive impact of non-antibiotic drugs on human gut bacteria. *Nature* 2018;**555**:623−8.